International Journal of Nanomedicine

Dovepress
open access to scientific and medical research

Open Access Full Text Article

ORIGINAL RESEARCH

Targeted Delivery of Macrophage Membrane Biomimetic Liposomes Through Intranasal Administration for Treatment of Ischemic Stroke

Tianshu Liu, Mengfan Zhang, Jin Zhang, Naijin Kang, Linlin Zheng, Zhiying Ding

School of Pharmaceutical Sciences, Jilin University, Changchun, 130021, People's Republic of China

Correspondence: Zhiying Ding, School of Pharmaceutical Sciences, Jilin University, Changchun, 130021, People's Republic of China, Tel/Fax +86 13843180286, Email dzy@jlu.edu.cn

Purpose: Ginsenoside Rg3 (Rg3) and Panax notoginseng saponins (PNS) can be used for ischemic stroke treatment, however, the lack of targeting to the ischemic region limits the therapeutic effect. To address this, we leveraged the affinity of macrophage membrane proteins for inflamed brain microvascular endothelial cells to develop a macrophage membrane-cloaked liposome loaded with Rg3 and PNS (MM-Lip-Rg3/PNS), which can precisely target brain lesion region through intranasal administration.

Methods: MM-Lip-Rg3/PNS was prepared by co-extrusion method and was performed by characterization, stability, surface protein, and morphology. The cellular uptake, immune escape ability, and blood-brain barrier crossing ability of MM-Lip-Rg3/PNS were studied in vitro. The in vivo brain targeting, biodistribution and anti-ischemic efficacy of MM-Lip-Rg3/PNS were evaluated in MACO rats, and we determined the diversity of the nasal brain pathway through the olfactory nerve blockade model in rats. Finally, the pharmacokinetics and brain targeting index of MM-Lip-Rg3/PNS were investigated.

Results: Our results indicated that MM-Lip-Rg3/PNS was spherical with a shell-core structure. MM-Lip-Rg3/PNS can avoid mononuclear phagocytosis, actively bind to inflammatory endothelial cells, and have the ability to cross the blood-brain barrier. Moreover, MM-Lip-Rg3/PNS could specifically target ischemic sites, even microglia, increase the cumulative number of drugs in the brain, improve the inflammatory environment of the brain, and reduce the infarct size. By comparing olfactory nerve-blocking rats with normal rats, it was found that there are direct and indirect pathways for nasal entry into the brain. Pharmacokinetics demonstrated that MM-Lip-Rg3/PNS exhibited stronger brain targeting and prolonged drug half-life.

Conclusion: MM-Lip-Rg3/PNS might contribute to the accumulation of Rg3 and PNS in the ischemic brain area to improve treatment efficacy. This biomimetic nano-drug delivery system provides a new and promising strategy for the treatment of ischemic stroke.

Keywords: macrophage-membrane coating, biomimetic liposome, brain targeting, ischemic stroke, intranasal delivery

Introduction

Ischemic stroke is mainly caused by cerebrovascular occlusion. It has the high incidence, mortality, and disability rate, which seriously affect human health and economic development. At present, the treatment of ischemic stroke mainly involves surgical intervention, which can clear intravascular thrombosis but still carries the risk of causing cerebral hemorrhage,[1] Alternatively, intravenous injection of recombinant tissue plasminogen activator (rt-PA), a widely recognized thrombolytic drug, is used,[2] However its treatment window is very narrow, and it may lead to neurotoxicity with significant toxic side effects.[3] In addition, recanalization of blood vessels can cause reperfusion injury, which increase oxidative stress and the release of pro-inflammatory factors, resulting in more serious damage.[4] Therefore, it is necessary to identify effective methods to reduce the damage caused by stroke and improve quality of life and survival rates.

The treatment of central nervous system diseases through intranasal administration has garnered considerable attention.[5,6] Unlike oral administration, intranasal administration can bypass the first pass effect of the liver, thereby increasing drug delivery efficiency into the brain,[7,8] Meanwhile, compared to intravenous administration, intranasal administration is non-invasive and can alleviate patient pain, with safety and convenience.[9,10] Intranasal administration

Received: 9 January 2024
Accepted: 10 June 2024
Published: 19 June 2024

Graphical Abstract

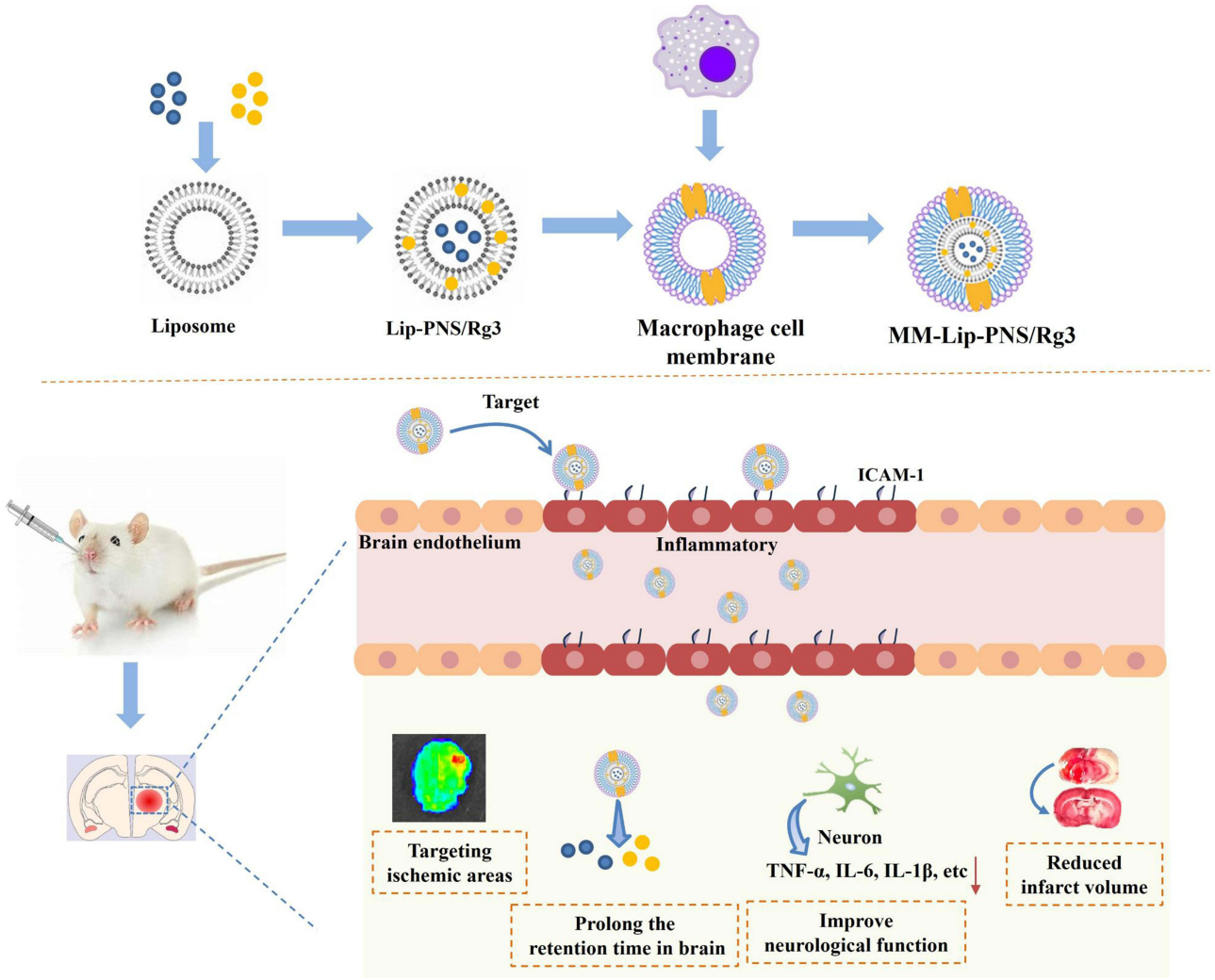

targets the brain through two pathways, Firstly, drugs can enter the brain directly and quickly through the trigeminal and olfactory nerve pathways. In addition, it can also enter the brain through an indirect pathway, that is, when the drug enters the nasal cavity, it enters the systemic circulation through the nasal respiratory mucosa and needs to cross the (blood-brain barrier) BBB before entering the brain.[5,11] To increase the delivery efficiency of drugs to the brain, it is necessary to explore a new type of nanomedicine. After intranasal administration, it can enter the brain through neural pathways. At the same time, it can also effectively cross the BBB, increase the amount of entry into the brain through indirect pathways and thus improving treatment effectiveness.

Panax notoginseng saponins (PNS) inhibit platelet aggregation, increase cerebral blood flow,[12,13] and reduce brain oedema.[14] Therefore, they can reduce damage after an ischemic stroke and are widely used to treat cerebral infarction.[15] Ginsenoside Rg3 (Rg3) exerts anti-inflammatory effects by inhibiting the production of pro-inflammatory factors while reducing oxidative stress reactions,[16,17] which can have a protective effect on the brain during cerebral ischemia.[18] Both PNS and Rg3 exert synergistic effects in ischemic stroke treatment. However, because of the presence of the BBB, it is difficult for Rg3 and PNS to enter the brain, which limits their therapeutic effect. Furthermore, these two drugs exhibit contrasting solubility; PNS is water soluble, whereas Rg3 is insoluble in water and has high non-polarity, complicating combined administration. Therefore, new drug delivery drug delivery system is required to overcome these problems.

Liposomes, resembling biofilms, are bilayer spherical vesicles formed by lipids and exhibit good biocompatibility.[19] Because of their unique bilayer structure, they can effectively carry drugs with diverse properties.[20] Hydrophilic drugs can be encapsulated in hydrophilic cores, while lipophilic drugs can be encapsulated in hydrophobic lipid bilayers, ultimately forming drug codelivery nanosystems.[21,22] These nanosystems can be used to improve drug bioavailability and reduce the need for repeated drug administration. However, liposomes do not target ischemic brain regions, making it difficult to deliver drugs accurately to the affected areas.

In recent years, biomimetic drug delivery systems have emerged as a promising technology for the treatment of diseases.[23] These systems utilize living cells or cell membranes to encapsulate nanoparticles and deliver them together as a whole, providing long-term blood circulation and disease-targeting properties.[24,25] However, there are still some shortcomings in using living cells as carriers. This is mainly because biological enzymes in living cells can affect the structure of nanoparticles inside the core, leading to drug leakage. Leaked drugs can also reduce the activity of living cells, which affect each other and are not conducive to the stability of biomimetic nanoformulations.[26,27] The cell membrane carrier system avoids this problem. It inherits the biological characteristics of living cells, retains surface proteins, and does not affect the nanoparticles in the core.[28,29] Biomimetic nanosystems based on cell membranes can disguise themselves as cells of the body, evading immune system detection, preventing engulfment, and prolonging circulation time.[30] Simultaneously, nanoparticles can be targeted to lesions by using different cell membrane coatings.[23,31] Ischemic stroke is often accompanied by an inflammatory reaction. Inflamed endothelial cells overexpress ICAM-1 protein, which specifically binds to CD11b on macrophages.[32,33] During cerebral ischemia, macrophages are rapidly recruited to the ischemic sites in the brain.[34,35] Therefore, it can be inferred that the nano-drug delivery system coated with macrophage membranes can target inflammatory endothelial cells in the brain after cerebral ischemia, aggregating towards brain damage.

In this study, we designed a biomimetic cell membrane nano-drug delivery system consisting of macrophage membrane-coated Rg3 and PNS double-loaded liposomes (MM-Lip-Rg3/PNS) that were used to target inflammatory brain endothelial cells for targeted therapy. We evaluated the immune escape ability of MM-Lip-Rg3/PNS, its affinity for brain endothelial cells. In addition, the in vivo pharmacokinetics, targeting of cerebral ischemic regions, and therapeutic effects of MM-Lip-Rg3/PNS were studied. The designed biomimetic liposomes exhibited good inflammatory reactivity and effectively protected damaged brain tissue, offering a promising new strategy for the treatment of ischemic stroke.

Materials and Methods

Materials

Egg yolk phosphatidylcholine (LIPOID E80) was supplied by Lipoid, Germany. Cholesterol was purchased from Guangfu Fine Chemical Research Institute (Tianjin, China). Panax notoginseng saponins (PNS) was purchased from Nanjing Dilger Medical Technology. Ginsenoside Rg3(Rg3) was supplied by Ytbiopharm (Changchun, China). Rhodamine B (RhB) was purchased from Adamas (Shanghai, China).1,1'-Dioctadecyl-3,3,3',3'-Tetramethylindodicarbocyanine,4-Chlorobenzenesulfonate Salt (DiD) was purchased from Celarts (Changchun, China). Chloroform was purchased from Chengdu Chron Chemical Co., Ltd. (Chengdu, China). Acetonitrile was purchased from Fisher Scientific (New York, USA). Methanol was purchased from YUHE New Mat (Shandong, China).

Cell Culture and Animals

The mouse monocyte-macrophage cell line RAW264.7 was purchased from Pricella Bioscience Inc. (Wuhan, China). RAW264.7 cells were cultured in DMEM supplemented with 10% foetal bovine serum (FBS). Human cerebral microvessel endothelial cell/D3 (hCMEC/D3) is a cell line derived from the human brain that grows in the BBB, making it suitable for establishing BBB models in in vitro experiments. hCMEC/D3 cells were purchased from Deltabio Inc. (Chengdu, China), and were cultured in an endothelial cell medium supplemented with 5% FBS, 1% cell growth factors, and 1% penicillin/streptomycin (ScienCell, USA). Two types of cells were cultured in a constant temperature incubator at 37°C with 5% CO2.

Sprague Dawley (SD) rats were purchased from Changchun Yisi Experimental Animal Technology Co., Ltd. (Changchun, China). All animal experiments were conducted in accordance with the guidelines evaluated and approved by the Ethics Committee of Jilin University.

Preparation of Rg3 and PNS Co-Loaded Liposomes

Lip-Rg3/PNS was prepared using a thin-film dispersion method.[36] First, different weights of egg yolk lecithin, cholesterol, and Rg3 were placed in a chloroform–methanol (2:3) solution. After ultrasonic dissolution, the organic solvent was slowly removed using a rotary evaporator at 37°C to form a uniform lipid film in a pear-shaped flask. Subsequently, PNS aqueous solution was added to hydrate the dry film, sonicated for 10 min using a probe in an ice bath, and passed through a 0.22 μm microporous filter membrane to obtain Lip-Rg3/PNS.

Macrophage Membrane Extraction

Logarithmic growth stage macrophages were scraped from the culture bottle using a cell scraper and transferred to a centrifuge tube. An ultrasonic cell crusher was used to break the cell suspension at 200 w, and the entire process was performed in an ice water bath. The obtained cell lysate was centrifuged at 1000 rpm for 10 min at 4°C, and the precipitate was removed. The supernatant was centrifuged at 12, 000 rpm for 20 min to form macrophage membranes (MM).

Preparation and Characterization of MM- Lip-Rg3/PNS

The Lip-Rg3/PNS liposomes were added to the MM membrane solution and treated with an ultrasound probe for 1 min in an ice bath. The resulting mixture underwent extrusion with a liposome extruder to obtain macrophage membrane-disguised biomimetic liposomes (MM-Lip-Rg3/PNS).

Characterization of Liposomes

The particle size, polydispersity index (PDI), and zeta potential of Lip-Rg3/PNS and MM-Lip-Rg3/PNS were measured using Dynamic Light Scattering (DLS) (Malvern Instruments, UK). Transmission electron microscopy (TEM) (Tecnai Spirit Biowin, Netherlands) was used to observe the morphology of MM-Lip-Rg3/PNS. The Lip-Rg3/PNS and MM-Lip-Rg3/PNS was stored at 4°C and room temperature for 14 days. The measured particle size at a given time interval to analyze stability.

Free Rg3 and PNS were removed using low-speed centrifugation and ultracentrifugation, respectively. The total amount of the drug and the amount of encapsulated drug were measured, and the encapsulation efficiency (EE) and drug loading (DL) were calculated. MM-Lip-Rg3/PNS and Lip-Rg3/PNS were stored at 4°C and 37°C, and their particle size and PDI values were measured for 7 consecutive days to evaluate their stability. The formula for the EE% and DL% were as follow:

$$\mathrm{EE\%} = \frac{\textit{Amount of encapsulated drug}}{\textit{Amount of total drug}} \times 100\%$$

$$\mathrm{DL\%} = \frac{\textit{Weight of encapsulated drug}}{\textit{Weight of Liposome}} \times 100\%$$

SDS-PAGE and Western Blotting

Membrane proteins in MM, Lip-Rg3/PNS, and MM-Lip-Rg3/PNS were extracted using radioimmunoprecipitation assay (RIPA) lysis buffer and separated using 10% SDS-PAGE (Epizyme Biotechnology), and stained with Coomassie brilliant blue (SevenBio) to observe protein bands.

Each protein sample was separated using 10% SDS-PAGE and transferred onto polyvinylidene fluoride membranes. After blocking with blocking solution, membranes were incubated overnight at 4°C with primary antibodies, including CD47 (Zenbio) and CD11b (Zenbio). The sections were then incubated with a horseradish peroxidase-conjugated secondary antibody (Zenbio). Finally, an enhanced chemiluminescence detection kit (Seven Bio) was used to detect the bands.

In vitro Inflammatory Response of MM-Lip-Rg3/PNS

HCMEC/D3 cells were stimulated with 0.5, 1, 2, 4, 6, and 8 μg/mL lipopolysaccharide (LPS) for 3 h, and the cell survival rate was measured using the cell counting kit-8 (CCK-8) method. The selected LPS concentration had a slight impact on the cell survival rate when stimulating hCMEC/D3 cells for 3 h. Flow cytometry was used to detect the expression of ICAM.

Approximately 8×10^4 hCMEC/D3 cells/well were seeded onto a laser confocal disc and cultured for 24 h. After stimulating cells with 1μg/ mL LPS for 3 h, Lip-RhB and MM-Lip-RhB (the concentration of RhB in each well was 10.0 μg/mL) were added. After incubation for 3 h, the cells were washed thrice with PBS, stained with DAPI, and examined using a laser confocal microscope (CLSM).

Immune Escape Ability

RAW264.7 macrophage cells were evenly seeded onto a laser confocal disc at a density of 2×10^5 cells per well and then incubated with Lip-RhB and MM-Lip-RhB in the dark for 3 h. After staining with DAPI, CLSM was used for observation.

RAW264.7 macrophage cells were seeded in a 6-well plate at a density of 2×10^5 cells per well and incubated with Lip-RhB and MM-Lip-RhB in the dark for 3 h. After washing with PBS, the cells were gently scraped off and collected, and fluorescence intensity was measured using flow cytometry.

In vitro Cytotoxicity

CCK-8 assay was performed to evaluate the effects of Rg3/PNS, Lip-Rg3/PNS, and MM-Lip-Rg3/PNS on hCMEC/D3 cells. HCMEC/D3 cells were seeded in 96-well plates at a density of 1×10^4 cells/well. Rg3/PNS, Lip-Rg3/PNS, and MM-Lip-Rg3/PNS with concentrations of 3, 5, 10, 20, 40, 60, and 100 μg/mL (Rg3 concentration) were added to the cells. After hCMEC/D3 cell incubation for 24 h, CCK-8 solution was added to each well and incubated at 37°C and 5% CO2 for 2 h. The optical absorbance density was measured using a microplate reader at 450 nm.

The Effect of Efflux Proteins on BBB Transport

To study the impact of efflux proteins on liposome entry into cells, efflux protein inhibitors (verapamil, ko143, and MK571) corresponding to P-glycoprotein (P-gp), cancer resistance protein (BCRP), and multidrug resistance-associated protein (MRP) on the BBB were used. Briefly, 3×10^5 hCMEC/D3 cells were seeded in a 6-well plate. After incubating cells with verapamil (20 μM), ko143 (3 μM), and MK571 (20 μM) for 1 h, the culture medium was discarded, and normal culture media containing Rg3/PNS, Lip-Rg3/PNS, and MM-Lip-Rg3/PNS (Rg3 concentration was all 50 μg/mL) were added for continued incubation for 3 h. The cells were lysed and centrifuged, and the supernatant was analysed for Rg3 and PNS content using HPLC.

In vitro BBB Transwell Assay

The hCMEC/D3 cells were seeded in the upper chamber of the Transwell (0.4 μm, Labselect). The transepithelial/ endothelial electrical resistance (TEER) value was measured, and when it reached 200 Ω·cm2, it was considered that the establishment of the BBB model had been successful. Medium containing or without LPS was added to the lower chamber, and Rg3/PNS, Lip-Rg3/PNS, and MM-Lip-Rg3/PNS (all with an Rg3 concentration of 50 μg/mL) were added to the upper chamber. After 12 h of cultivation, the lower chamber culture medium was collected to determine the Rg3 and PNS content.

Animals

Sprague Dawley (SD) rats were selected as experimental animals and purchased from Changchun Yisi Experimental Animal Technology Co., Ltd. (Changchun, China). All animal procedures were performed in compliance with the China National Institute's Guidelines on the Care and Use of Laboratory and were approved by the Animal Experimental Ethics Committee of Jilin University (Approval No. 20210069).

Olfactory Nerve Blockade Experiment

An olfactory nerve blockade model was established to study the pathway by which macrophage membrane-coated liposomes enter the brain after intranasal administration. Rats were anaesthetized with an intraperitoneal injection of 2% sodium pentobarbital. Fix the rat head with a brain stereotaxic apparatus, adjust the parameters: AP: +8 mm, ML: ± 2 mm, insert a flexible Teflon blade at the intersection, and cut off all olfactory axons, after the surgery, suture the incision. The olfactory nerve blockade model group and the normal group rats were administered MM-Lip-DiD (0.38 μg DiD/kg body weight) through the nose. After 1 h of administration, IVIS spectroscopy was used for fluorescence optical imaging. Subsequently, the brains were isolated from the sacrificed rats for in vitro fluorescence distribution, and the fluorescence intensity was quantified using IVIS spectroscopy.

Middle Cerebral Artery Occlusion (MCAO) Model

Rats were anesthetized using 1% sodium pentobarbital and carefully dissected to expose the common carotid artery (CCA), external carotid artery (ECA), and internal carotid artery (ICA). An incision was made in the ECA, and a nylon thread was inserted from the incision into the ICA for approximately 8–10 mm, effectively blocking the origin of the middle cerebral artery.

In vivo Imaging of MCAO Rats

To verify whether ischemic brain endothelial cells express ICAM-1, immunofluorescence staining was performed. After administering MM Lip DiD in the nasal cavity for 4 hours, brain tissue was isolated, fixed, and sliced to observe the expression of ICAM-1.

After 24 h of MCAO, rats were administered MM-Lip-DiD (0.32 μg DiD/g), and brain fluorescence was observed using an IVIS Spectrum imaging system at 0.5, 1, 4, 12, and 24 h.

MCAO rats were randomly divided into three groups: free DiD, Lip-DiD, and MM-Lip-DiD, and nasally administered at a dose of 0.32 μg DiD/g. After 4 h, the rats were sacrificed for brain, heart, liver, lungs, kidneys, and spleen analyses. Fluorescence intensity was quantified using the IVIS Spectrum imaging system.

Fluorescence Co-Localization of MM-Lipo and Microglia

MCAO rats were sacrificed after 4 h of nasal administration of MM-Lip-DiD. The brains were collected and fixed in paraformaldehyde, dehydrated and then frozen into sections. The sections were incubated overnight at 4 °C in Iba-1 primary antibody, washed with PBS three times, and incubated with secondary antibody at 37 °C for 1 h. Finally, the sections were imaged under CLSM.

Pharmacokinetics and Brain Targeting Analysis

Rats were randomly divided into three groups and given free drugs (Rg3/PNS), drug-loaded liposomes (Lip-Rg3/PNS), and drug-loaded liposomes coated with MM membranes (MM-Lip -Rg3/PNS) at an equal dose of 3.6 mg/kg Rg3 and 13.2 mg/kg PNS. Blood was collected at various time points (0.03, 0.08, 0.16, 0.25, 0.5, 1, 2, 4, 6, 8, 12, 24, and 48 h). Plasma was collected after centrifugation at 4000 rpm for 10 min. Brain tissue was collected and washed with physiological saline. Physiological saline was added to homogenise brain tissue, and the brain homogenate or plasma was mixed with methanol and vortexed for 2 min to remove proteins. The supernatant was collected, and ethyl acetate was added to the precipitate before vortexing again for 2 min. The supernatant was collected after centrifugation, and the two supernatants were combined, dried with nitrogen, and dissolved in 0.5 mL methanol for content determination.

Pharmacokinetic parameters were calculated using DAS 3.0. The relevant targeting index was calculated based on the obtained pharmacokinetic parameters, including targeting efficiency (Te), relative uptake rate (Re), peak concentration ratio (Ce), and drug targeting index (DTI%). Te, Ce, Re, DTI values were calculated as follows:

$$\mathrm{Te} = (AUC_{(0-t)})_{brain} / (AUC_{(0-t)})_{plama}$$

$$\mathrm{Ce} = (C_{max})_{Liposome}/(C_{max})_{Rg3/PNS}$$

$$\mathrm{Re} = (AUC_{(0-t)})_{Liposome}/(AUC_{(0-t)})_{Rg3/PNS}$$

$$\mathrm{DTI\%} = \frac{(AUC_{brain}/AUC_{plama})_{Liposome}}{(AUC_{brain}/AUC_{plama})_{Rg3/PNS}} \times 100\%$$

Cerebral Oedema and Cytokine Measurement

After 14 d of treatment for MCAO rats, the brains were removed from the sacrificed rats, and the brain wet weight was measured (A1). The weighed brains were placed in a 60°C oven, dried for 48 h, and weighed as brain dry weight (A2). The water content of brain tissue was calculated using the following formula:

$$\text{Brain water content}\,(\%) = (A1 - A2)/A1 \times 100\%$$

The brain, ground with PBS, underwent ELISA for IL-1β, IL-6, and TNF-α content using ELISA kits (Jianglai Biology, China).

Cerebral Infarction Area Assessed with TTC

Model rats were treated with different formulations for 14 d. The rats were randomly divided into five groups, including a sham group and four model groups. After 14 d of intranasal administration with saline, Rg3/PNS, Lip-Rg3/PNS, and MM-Lip-Rg3/PNS, brain tissue was dissected into 2 mm thick coronal sections and frozen at –20°C. Brain sections were stained with 1% 2,3,5-TTC solution in the dark for 30 min. The infarcted area was represented by areas without red staining. The infarct size was quantified using ImageJ software.

In vivo Safety Evaluation

The rats were sacrificed after administering different formulations for 14 days, and sliced the brain, heart, lung, liver, spleen, and kidney for H&E staining and tissue structure analysis.

Statistical Analysis

All assays were independently repeated at least thrice. All data were presented as mean ± standard deviation (SD). Statistical analysis was performed using one-way analysis of variance, and the results were considered statistically significant when the p-value was < 0.05.

Results and Discussions

Preparation and Characterization of MM-Lip-Rg3/PNS

A film dispersion method was used to prepare Lip-Rg3/PNS.[36] Particle size, PDI, and zeta potential of Lip-Rg3/PNS were investigated using DLS (Figure 1A and B). The particle size of the Lip-Rg3/PNS was 157.9±0.66 nm. The PDI of Lip-Rg3/PNS was 0.154±0.012, indicating that the liposomes had high dispersibility and good uniformity. The zeta potential of Lip-Rg3/PNS was –10.57 ± 0.45mV. The EE values of Rg3 and PNS were 91.87±1.30% and 83.33±0.34% in Lip-Rg3/PNS, respectively. The DL values of Rg3 and PNS were 2.83±0.04% and 9.85±0.04% in Lip-Rg3/PNS, respectively.

The preparation of MM-Lip-Rg3/PNS is illustrated in Figure 1A. The cell membrane of RAW264.7 cells was extracted using ultrasonication, and Lip-Rg3/PNS was co-extruded with the macrophage membrane to form macrophage membrane-coated double-loaded liposomes. The cell membrane protein weight-to-phospholipid ratio was optimized by measuring changes in zeta potential and particle size.[37] As shown in Figure 1D, the particle size of MM-Lip-Rg3/PNS gradually increased with the addition of membrane proteins. The zeta potential results showed that after the phospholipids-to-cell membrane protein weight ratio of 2.5:1, the zeta potential of MM-Lip-Rg3/PNS remained nearly constant and closely approached the potential of the cell membrane, registering a zeta potential value of –21.5 ± 1.11mV. DLS

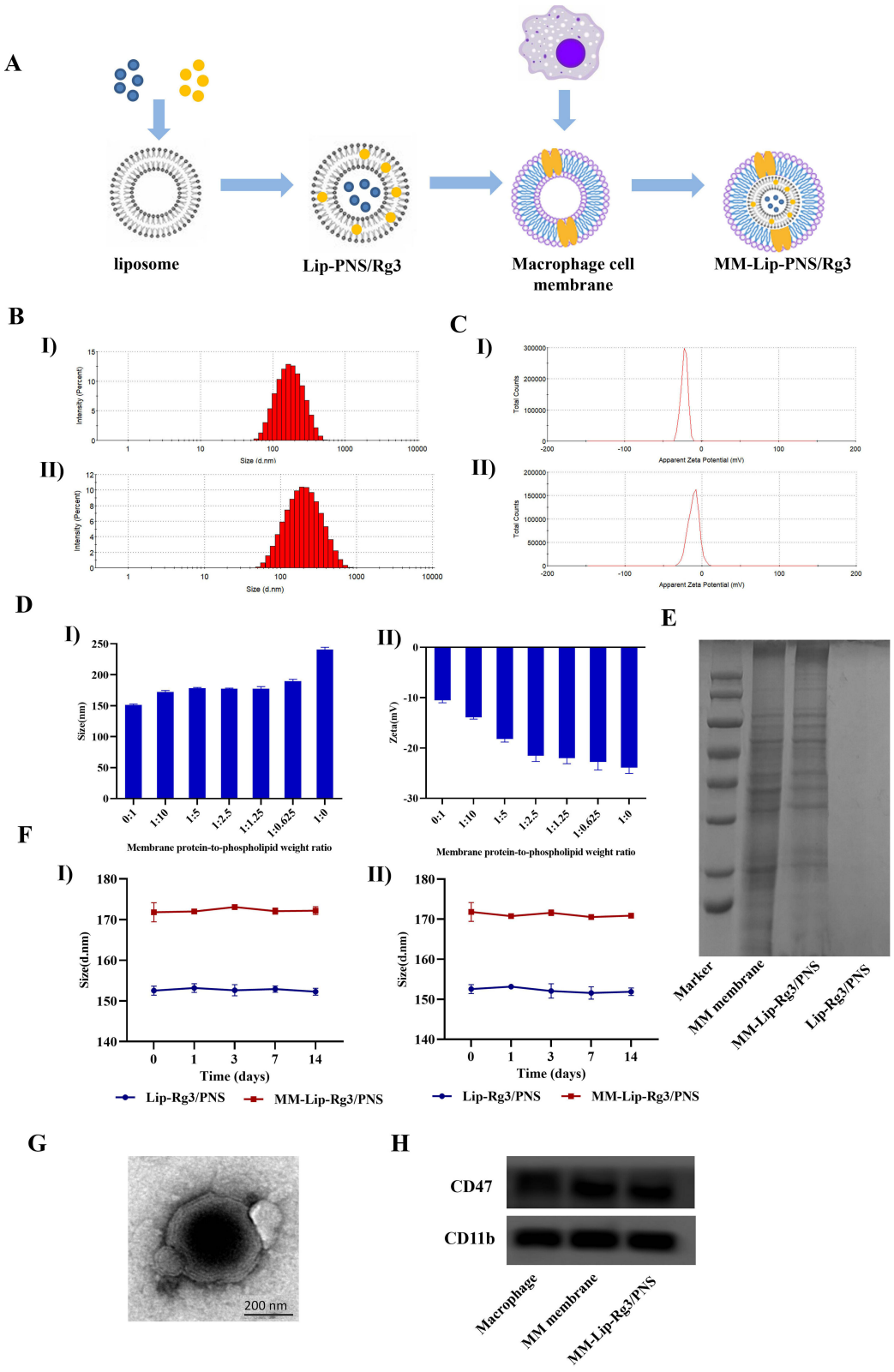

Figure 1 Preparation and characterization of MM-Lip-Rg3/PNS. (**A**) Schematic preparation of RVG/TPP-MASLNs-GS. (**B**) Particle size of (I) Lip-Rg3/PNS and II) MM-Lip-Rg3 /PNS. (**C**) Zeta potential of (I) Lip-Rg3/PNS and II) MM-Lip-Rg3/PNS. (**D**) Particle size and zeta potential of MM-Lip-Rg3/PNS with different ratios of membrane proteins to phospholipids ratios. (I) particle size, II) zeta potential. (**E**) Proteins in macrophage membrane, MM-Lip-Rg3/PNS, and Lip-Rg3/PNS, analyzed with SDS-PAGE. (**F**) Size stability of Lip-Rg3/PNS and Lip-Rg3/PNS at (I) 4°C and II) room temperature. (**G**) Representative TEM image of MM-Lip-Rg3/PNS. (**H**) Western-blot analysis of macrophages, macrophage membranes, and MM-Lip-Rg3/PNS for its surface characteristic protein (CD47, CD11b). Data are presented as means ± SD, n = 3.

analysis results showed the particle size of MM-Lip-Rg3/PNS was 177.7±0.70 nm (Figure 1B and C), which was approximately 20 nm higher than that of Lip Rg3/PNS, indicating that the macrophage membrane was successfully coated on the surface of the liposomes.[32] The results of transmission electron microscopy (TEM) also indicated the success of the coating. In addition, the PDI of MM-Lip-Rg3/PNS was 0.187 ± 0.009. By detecting the particle size of liposomes, it was found that there was no significant change within 14 days (Figure 1F), indicating good stability of MM-Lip-Rg3/PNS and Lip-Rg3/PNS.

Cell membrane proteins serve as the foundation for biological functions. The SDS-PAGE results showed that there were no protein bands present in Lip-Rg3/PNS, and the protein bands of MM-Lip-Rg3/PNS and the cell membrane were almost consistent (Figure 1E), indicating that MM-Lip-Rg3/PNS retained most of the macrophage membrane proteins. CD47 and CD11b are two characteristic functional proteins expressed on the macrophage membrane. CD47 prevents phagocytosis by the autoimmune system,[38] and CD11b recognizes inflammatory endothelial cells.[39] Western blot analysis showed that both proteins were expressed on MM-Lip-Rg3/PNS and macrophage membranes (Figure 1H).

MM-Lip-Rg3/PNS Bound to Inflammatory Endothelial Cells

To investigate the affinity of MM-Lip-Rg3/PNS for the inflamed endothelium, we used LPS to induce inflammation in hCMEC/D3cell to simulate the inflammatory environment in the brain during cerebral ischemia. We used the CCK-8 method to analyse the effects of different concentrations of LPS on hCMEC/D3 cell viability. As shown in Figure 2A, when the concentration of LPS was 1 μg/ mL, it had a certain impact on cell viability, and the cell survival rate was 86.99%. Therefore, LPS with a concentration of 1 μg/mL was selected for subsequent experiments. ICAM-1 is expressed after the activation of endothelial cells and can specifically bind to CD11b, a major protein that binds MM-Lip-Rg3/PNS to the endothelium.[40] After stimulating hCMEC/D3 cells with LPS (1 μg/mL), ICAM-1 was upregulated (Figure 2B). MM-Lip-Rg3/PNS or Lip-Rg3 /PNS were incubated with hCMEC/D3 cells for 6 h before and after LPS treatment. The CLSM images indicated that there was no significant difference in the aggregation of Lip-Rg3/PNS between inflammatory and non-inflammatory cells, and the fluorescence was weak. However, under inflammatory conditions, the binding of MM-Lip-Rg3/PNS to activated hCMEC/D3 cells was enhanced and exhibited strong fluorescence, while exhibiting weak fluorescence around non-inflammatory cells (Figure 2C). These results indicated that MM-Lip-Rg3/PNS had a strong affinity for the inflamed endothelium, whereas liposomes did not, suggesting an increased interaction between MM and the endothelium after inflammation.

Immune-Escape Function in vitro

To assess the immune escape capability of MM-coated liposomes, MM-Lip-RhB and Lip-RhB were incubated with RAW 264.7 cells for 6 h and observed with CLSM. As shown in Figure 3A, the relative fluorescence intensity observed in macrophages treated with Lip-RhB was stronger than that observed in the MM-Lip-RhB group, indicating that MM-Lip-RhB reduced macrophage absorption. Flow cytometry was used to quantitatively analyze the uptake of macrophages, and the results showed that the fluorescence intensity of the Lip-RhB group was 2.04 times higher than that of the MM-Lip-RhB group (Figure 3B and C). Both methods suggest that liposomes coated with MM inherit macrophage characteristics, impede elimination by the immune system, and sustain long-term circulation in the body.

The Effect of Efflux Inhibitors on the Transport of Liposomes

After incubating hCMEC/D3 cells with different concentrations of Rg3/PNS, Lip-Rg3/PNS, and MM-Lip-Rg3/PNS for 24 h, the cell survival rate was found to exceed 80%, indicating that Rg3/PNS, Lip-Rg3/PNS, and MM-Lip-Rg3/PNS were not toxic to hCMEC/D3 cells (Figure 4A). Efflux transporters such as P-gp, BCRP, and MRP are expressed in brain endothelial cells and can limit the absorption of drugs into the brain.[41,42] Therefore, we investigated the effects of these efflux transporters on the transport of Rg3 and PNS across the BBB. The results showed that compared with the Lip-Rg3/PNS and MM-Lip-Rg3 /PNS groups, the free Rg3/PNS group was most impacted by these three inhibitors (Figure 4D and E). After the addition of inhibitors, the cellular uptake of Rg3 and PNS in the Rg3/PNS group significantly increased, indicating that free Rg3 and PNS were transported through three types of efflux transporters. The low brain uptake of aqueous solutions of Rg3 and PNS may be related to their efflux effects on the hCMEC/D3 cell. The improvement in Rg3 and PNS in the Lip-Rg3/PNS and MM-Lip-Rg3/PNS groups was less than that in the Rg3/PNS group, particularly in the MM-Lip-Rg3/PNS group, showing the lowest

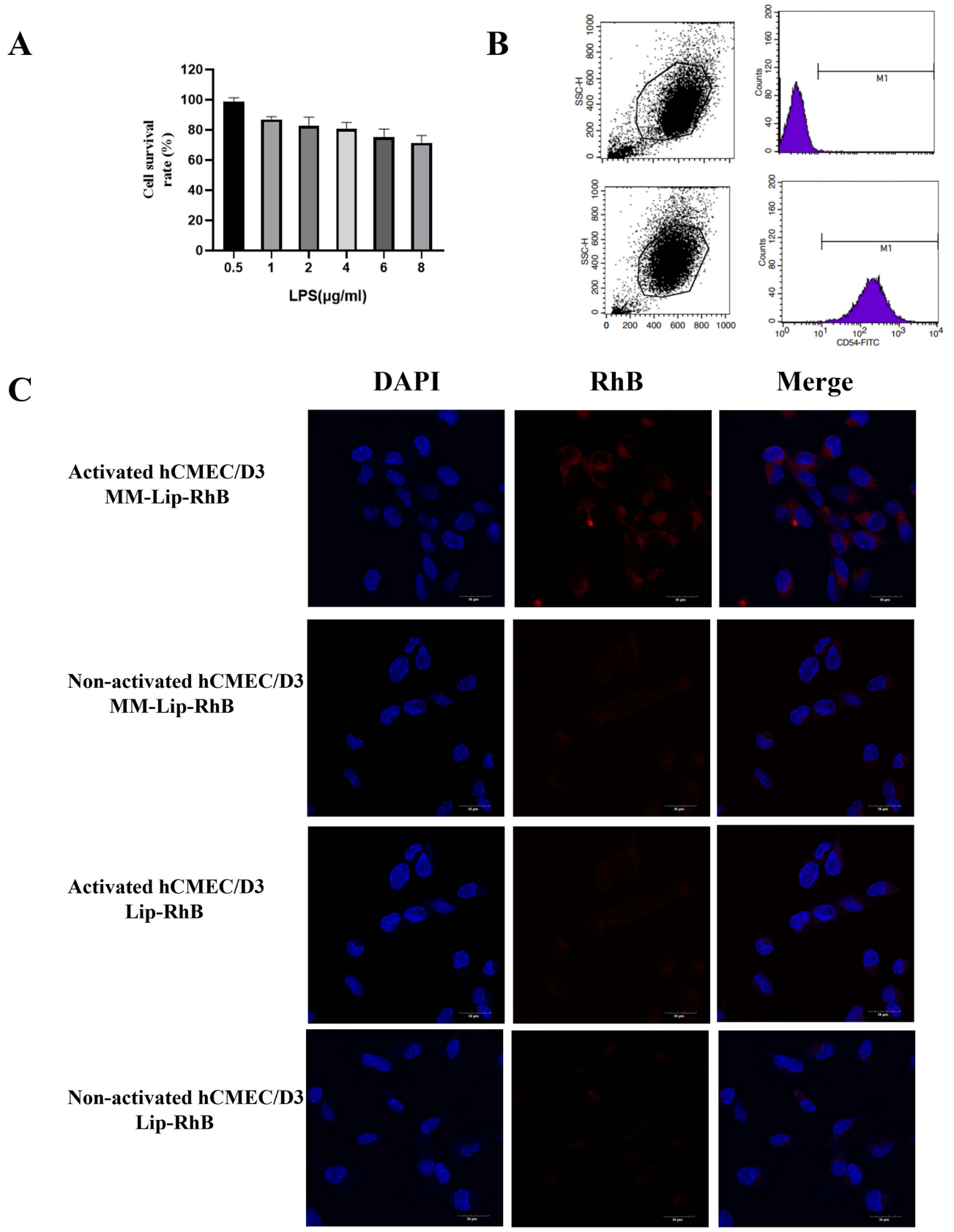

Figure 2 Inflammatory response and release profile of MM-Lipo in vitro. (**A**) The effect of LPS concentration on hCMEC/D3 cells survival rate. (**B**) ICAM-1 of hCMEC/D3 cells before and after LPS stimulation. (**C**) Fluorescence confocal images show the binding of DiD-labeled liposomes (red) to inflamed hCMEC/D3 cells stained by DAPI (blue). hCMEC/D3 cells were activated with LPS /without LPS (scalebar: 30 μm). The data were presented as the mean ± SD (n =3).

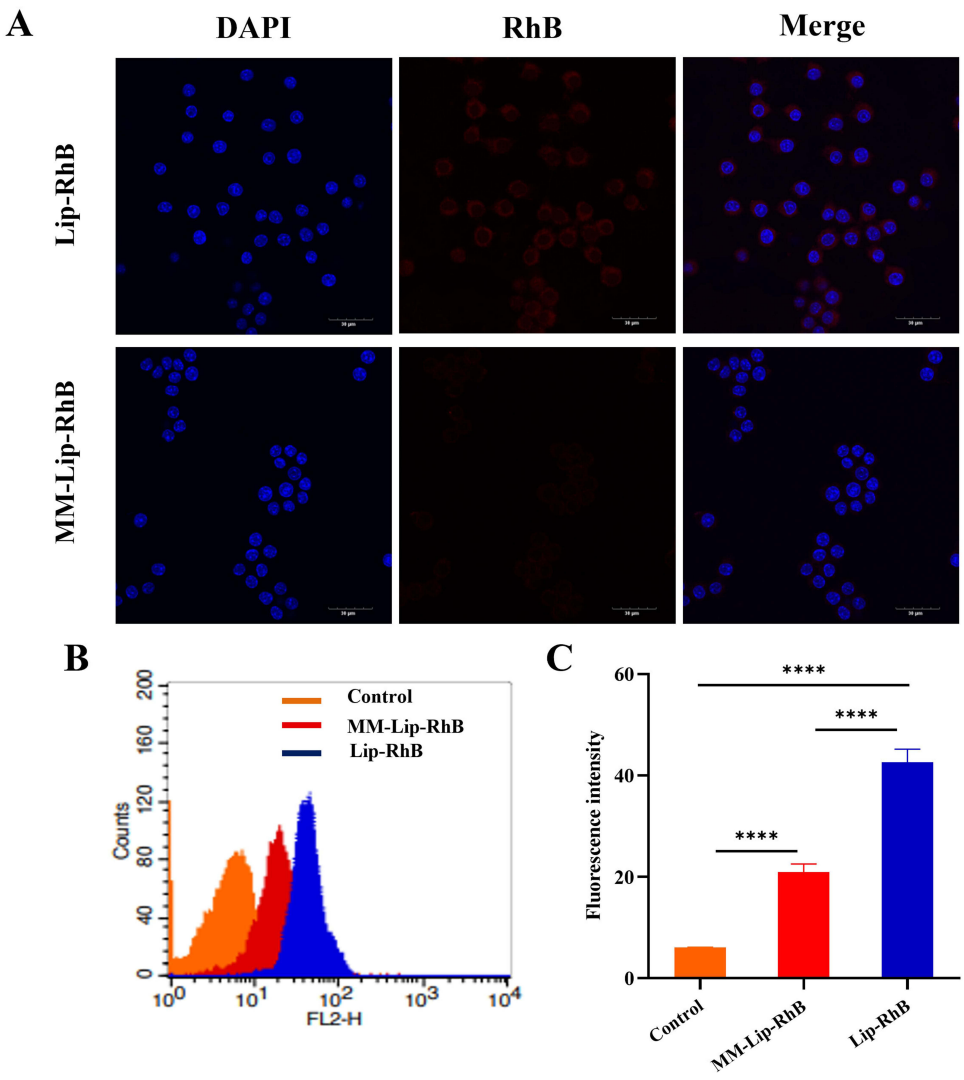

Figure 3 Immune-escape function in vitro. (**A**) Confocal laser microscope images of macrophages (blue) incubated with MM-Lip-RhB and Lip-RhB (red), (scale bar =30μm). (**B**) Cellular uptake of MM-Lip-RhB and Lip-RhB in macrophages by flow cytometry. (**C**) Quantification of the cellular uptake of MM-Lip-RhB and Lip-RhB in macrophages. The data were presented as the mean ± SD (n =3). ****p < 0.0001.

percentage of improvement. This suggests that efflux transporters had reduced transport capacity in the two formulation groups. It may be because liposomes encapsulate drugs internally, and their bilayer membranes, resembling biofilms, reduce recognition by efflux proteins. Additionally, MM-Lip-Rg3/PNS may avoid efflux due to the encapsulation of the cell membrane, leading efflux transporters to mistake it for a "self" substance.[43] Differences in the effects of the three efflux proteins on Rg3/PNS, Lip-Rg3/PNS, and MM-Lip-Rg3/PNS were observed. The ko143 inhibitor had the greatest impact on the intake of free PNS, whereas the MK571 inhibitor had the greatest impact on the intake of free Rg3. This indicates that the BCRP and MRP transporters may be the main efflux transporters in PNS and Rg3 aqueous solutions. In addition, the effects of the three inhibitors on the cellular uptake of Rg3 and PNS in liposomes were almost identical, indicating that both Rg3 and PNS were encapsulated within the liposomes and entered the cells as a whole with minimal leakage. Lip-Rg3/PNS was mainly discharged through the BCRP and MRP transporters, whereas MM-Lip-Rg3/PNS was mainly discharged through the P-gp and BCRP transporters.

Investigation of BBB Penetration Ability

Transwell assays were performed to establish an in vitro BBB model.[44,45] Cells were inoculated into the upper chamber of the T ranswell, and medium was added to the lower chamber (Figure 4B). After 4 d of cultivation, the TEER value could be stably

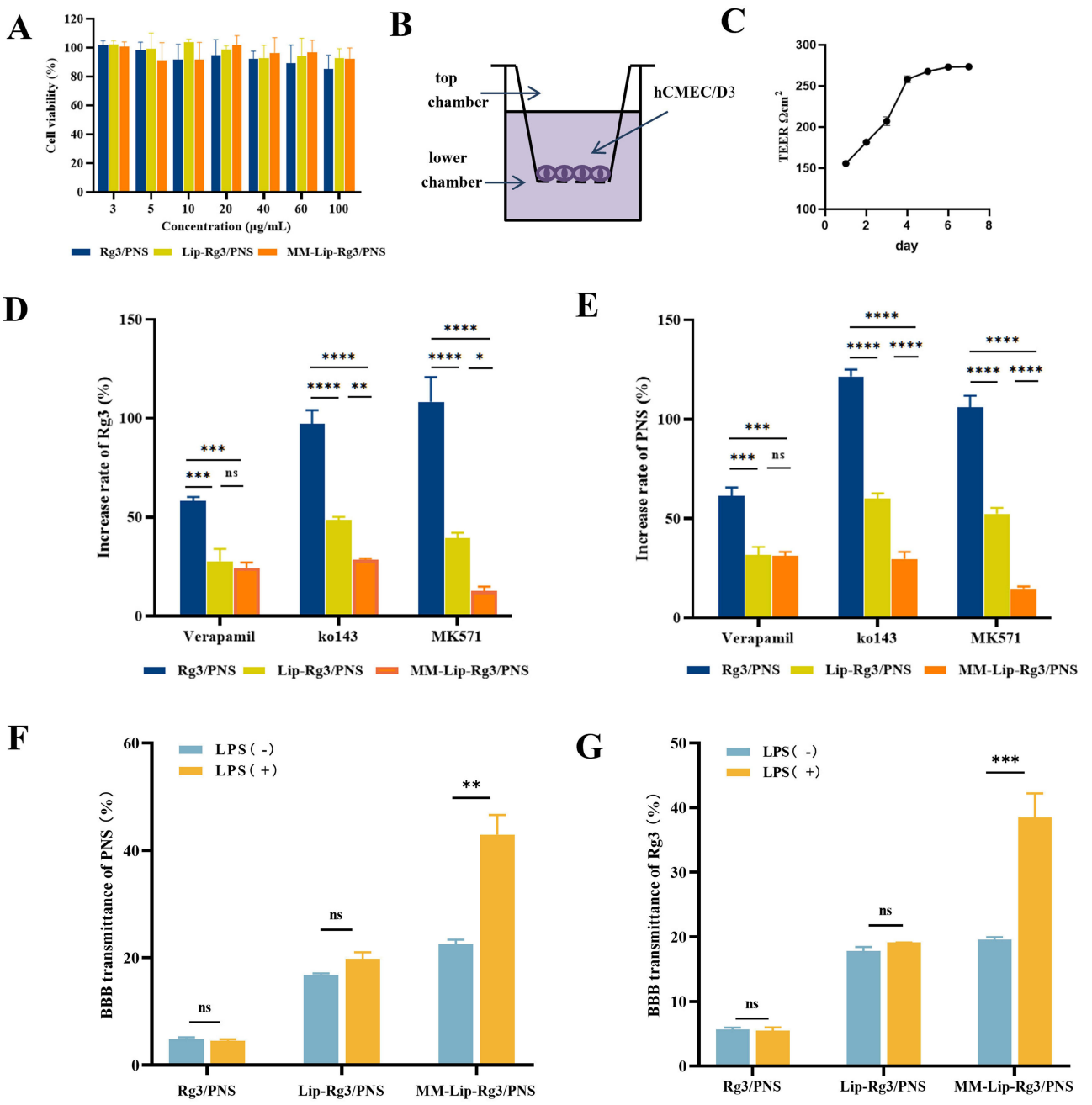

Figure 4 Efflux transporters on cellular uptake and BBB transmigration. (**A**) The cell viability of hCMEC/D3 cells after 24h treated with different concentrations of Rg3/PNS, Lip-Rg3/PNS, and MM-Lip-Rg3/PNS. (**B**) Schematic diagram of in vitro BBB model. (**C**) TEER value of BBB within 7 days. (**D**) hCMEC/D3 cells before and after treatment with efflux protein inhibitors were incubated with different formulations to determine the increase rate of PNS uptake. (**E**) hCMEC/D3 cells before and after treatment with efflux protein inhibitors were incubated with different formulations to determine the increase rate of Rg3 uptake. (**F**) The percentage of PNS crossing the BBB after incubation with different formulations, under LPS stimulation or non-stimulation conditions. (**G**) The percentage of Rg3 crossing the BBB after incubation with different formulations, under LPS stimulation or non-stimulation conditions. The data were presented as the mean ± SD (n =3). ****p < 0.0001, ***p < 0.001, **p < 0.01, *p < 0.05, ns no significant difference.

maintained at around 250 Ω cm2 (Figure 4C), indicating that the brain endothelial cells were tightly connected and the BBB model was successfully established.[46] We used LPS to induce inflammation to evaluate the ability of the MM-coated liposomes to cross the BBB under inflammatory conditions. In vitro migration experiments showed that, regardless of whether inflammation occurred (Figure 4F and G), the BBB transmittance of Rg3 and PNS solutions was very low. This indicated that the Rg3/PNS solution had difficulty entering the BBB. Under non-inflammatory conditions, no significant difference was observed in the ability of Lip-Rg3/PNS and MM-Lip-Rg3/PNS to penetrate the BBB. The transmittances of Rg3 were 17.79%

and 19.55%, and 16.79% and 22.5%, respectively. However, under inflammatory conditions, the transmittance of MM-Lip-Rg3/PNS was greatly improved, reaching 38.48% (Rg3) and 42.93% (PNS). The transmittance of Lip-Rg3/PNS did not change significantly, similar to that under non-inflammatory conditions, with 19.12% (Rg3) and 19.79% (PNS). Results indicated that LPS promoted the transmigration of MM-Lip-Rg3/PNS across the BBB, demonstrating its inflammatory responsiveness. After stroke, MM-Lip-Rg3/PNS penetrated the BBB.

Olfactory Nerve Blockade Experiment

A rat model of olfactory nerve blockade was established via surgical destruction of the olfactory bulb (Figure 5A and B).[47] As shown in Figure 5C, after administration, MM-Lip-DiD began to diffuse from the nasal cavity to the brain, and the intensity and ranges of DiD signals in the olfactory bulb-blocked model group was smaller than that in the normal group. After the rats were sacrificed, their brains were taken for quantitative analysis, and it was found that the fluorescence intensity in the brain of the normal group was higher than that of the model group (Figure 5D and E). The high fluorescence intensity in the normal group mean that MM-Lip-DiD was transported directly (through neural pathways) or indirectly (through systemic circulation) to the brain. After destroying the olfactory bulb, the model group could still detect fluorescence in the brain, indicating that some drugs still entered the brain. It was speculated that after the olfactory bulb was damaged, the "nose-brain" direct pathway was blocked, but the drug could still enter the brain through an indirect pathway. This part of the experiment proves that after drug absorption through the nose, it is likely to enter the brain through multiple pathways.

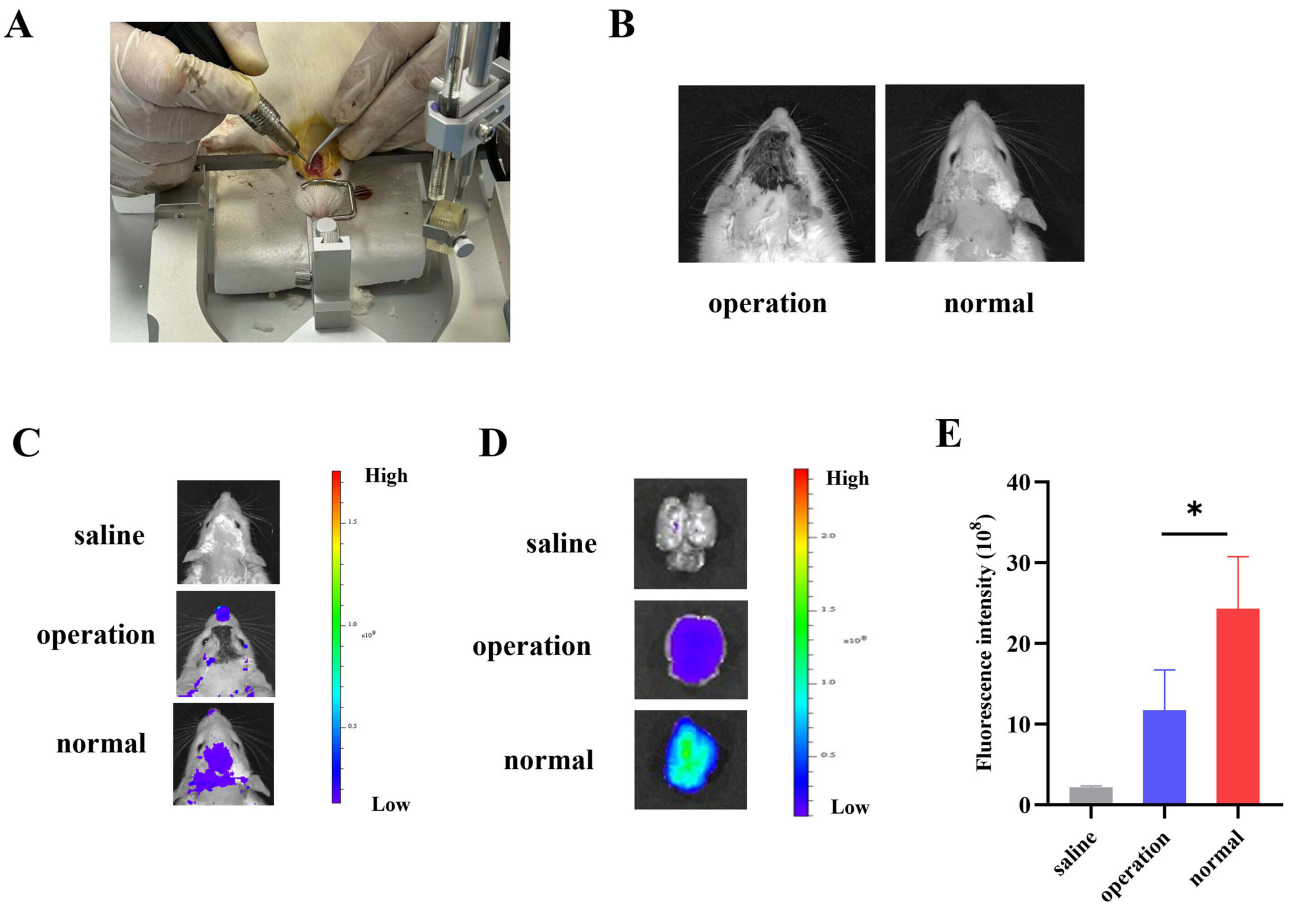

Figure 5 Observation of brain fluorescence after intranasal administration of MM-Lip-DiD formulations to olfactory nerve blockade model rats and normal rats. (**A**) Establishment of an olfactory nerve blockade model in rats. (**B**) Successfully modeled rats and normal rats. (**C**) Live imaging of MM-Lip-DiD distribution in the rat brain. (**D**) Ex vivo images of MM-Lip-DiD distribution in the rat brain. (**E**) Quantitative analysis of DiD fluorescence intensity in brain tissue. The data were presented as the mean ± SD (n =3). *p < 0.05.

In vivo Imaging of MCAO Rats

In the brain of MCAO rats, ICAM-1 was indeed expressed on the surface of endothelial cells, which was consistent with in vitro cell experiments, indicating that damaged brain endothelial cells will have ICAM-1 expression, providing a basis for MM-Lipo targeting the site of cerebral ischemic injury (Figure S1).

To verify the targeting effect of MM-coated liposomes on cerebral ischemic sites, DiD was loaded into MM-Lipo and administered nasally into MCAO rats (Figure 6A).[48] Fluorescence distribution was measured in the rat brains at 0.5, 1,4, 12, and 24 h after administration (Figure 6B). The results showed that fluorescence appeared in the brain at different time points, indicating that MM-Lipo has a long cycle. Moreover, the fluorescence intensity of the ischemic region (right

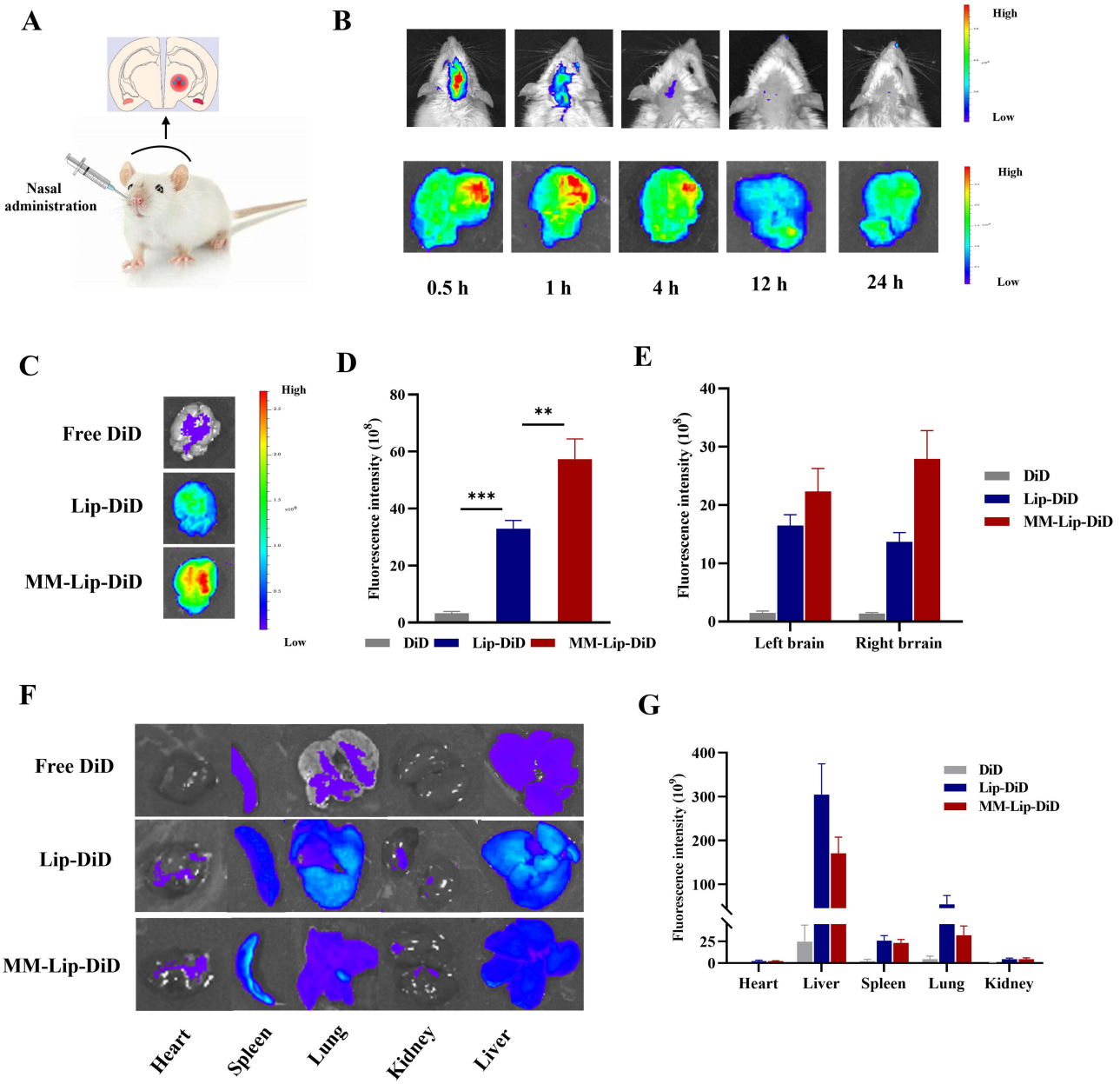

Figure 6 In vivo targeting research. (**A**) Schematic illustration of different preparations administered via the nose in MACO rats. (**B**) Live fluorescence imaging and ex vivo brain fluorescence images of MACO rats at 0.5, 1, 4, 12, and 24 hours after administration of MM-Lip-DiD. (**C**) EX vivo fluorescence imaging of brain of MACO rats that treated with free DiD, Lip-DiD and MM-Lip-DiD. (**D**) Quantitative analysis of DiD fluorescence intensity in brain tissue that treated with free DiD, Lip-DiD and MM-Lip-DiD. (**E**) Quantitative analysis of DiD fluorescence intensity of left and right brain. (**F**) EX vivo fluorescence imaging of heart, liver, spleen, lung and kidney of MACO rats that treated with free DiD, Lip-DiD and MM-Lip-DiD. (**G**) Quantitative analysis of DiD fluorescence intensity of heart, liver, spleen, lung and kidney. The data were presented as the mean ± SD (n =3). ***p < 0.001, **p < 0.01.

brain) was higher than that of the nonischemic region (left brain), suggesting that MM-Lipo tends to accumulate in the ischaemic hemisphere and targets the ischemic region of the brain.

In addition, free DiD, Lip-DiD, and MM-Lip-DiD were administered to MCAO rats to investigate the distribution of ordinary and MM-coated liposomes.[49] After 4 h, the rats were sacrificed, and the brain tissue was isolated for fluorescence quantification (Figure 6C). According to the results, it was found that MM-Lipo accumulated the most in the brain, with the fluorescence intensity in the MM-Lip-DiD group being 1.74 times higher than that in the Lip-DiD group and 17.59 times higher than that in the DiD group. The fluorescence intensity of MM-Lip-DiD in the ischemic right brain was higher than that in the left brain, and the fluorescence in the brain mainly accumulated in the ischemic area, while the fluorescence of Lip-DiD and DiD on both sides of the brain was almost indistinguishable (Figure 6D and E). These results are also consistent with those of previous studies. Following cerebral ischemia, the endothelial cells of the ischemic part of the brain express ICAM-1 protein, inducing an inflammatory response and targeting the ischemic site.[50,51] In contrast, bare liposomes lacked CD11b expression and did not exhibit targeted functionality. We further quantified the fluorescence in various tissues of the three groups of rats and observed that the fluorescence intensity of the liposome group in the liver was higher than that of the MM-Lip-DiD group (Figure 6F and G), which may be due to the ability of MM-Lipo to evade phagocytosis by the phagocytic system.[52]

Fluorescence Co-Localization of MM-Lipo and Microglia

After cerebral ischemia, microglia can quickly migrate to the lesion, participate in and mediate neuroinflammatory responses, and play an important role in the development of ischemic stroke. To further investigate whether MM-Lipo can target microglia, immunofluorescence analysis was performed on microglia after nasal administration of MM-Lip-DiD to MCAO rats to observe the co-localization of MM-Lip-DiD and microglia. As shown in Figure 7, it was found that MM-Lip-DiD exhibit good fluorescence co-localization with microglia, indicating that macrophage membrane biomimetic liposomes have a certain affinity for microglia and can target them after entering brain tissue, which provides a possibility for further regulating neuroinflammation.

Pharmacokinetics and Brain-Targeting Evaluation

To study the changes in drug concentration in vivo after the administration of Rg3/PNS, Lip-Rg3/PNS, and MM-Lip-Rg3/PNS, the drug concentrations were measured within 48 h (Figure 8). The two components with the highest content in the PNS, Rg1 and Rb1, were selected to represent PNS for subsequent analyses. According to the plasma concentration-time curve, free Rg3/PNS was rapidly eliminated from the blood, and Rg3 was not detected after 24 h, whereas Rg1 and Rb1 were not detected after 48 h. In the Lip-Rg3/PNS and MM-Lip-Rg3/PNS groups, these three components were still

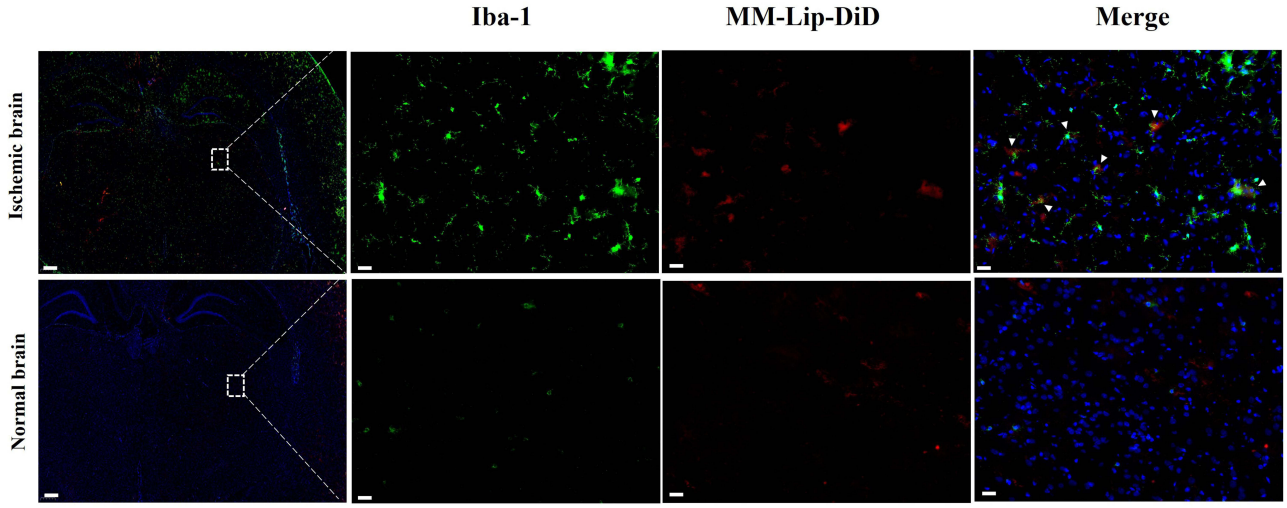

Figure 7 Fluorescence co-localization images of MM-Lip-DiD and microglia, Iba-1: green, MM-Lip-DiD: red, DAPI: blue (scale: 500/50 μm).

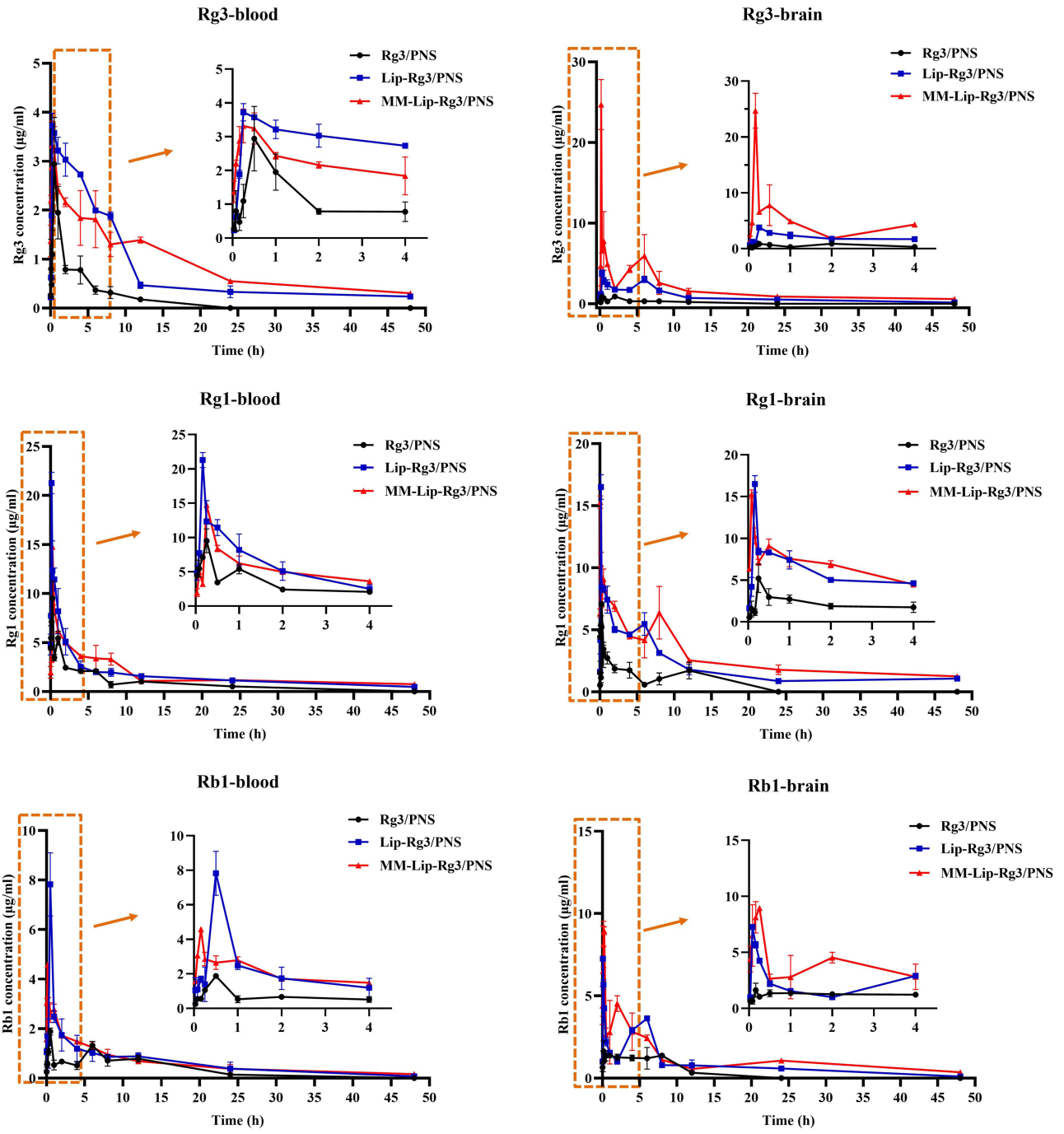

Figure 8 Concentration–time curve of Rg3, Rg1 and Rb1 in MACO rats after intranasal administration of Rg3/PNS, Lip-Rg3/PNS, and MM-Lip-Rg3/PNS. The data were presented as the mean ± SD (n =3).

detected after 48 h, indicating that Lip-Rg3/PNS and MM-Lip-Rg3/PNS prolonged the circulation time of drugs in the body. The pharmacokinetic parameters obtained by analyzing the blood drug concentration using DAS 3.0 are shown in Tables 1–3. The plasma pharmacokinetic parameters showed that the $t_{1/2}$ and MRT values for the Lip-Rg3/PNS and MM-Lip-Rg3/PNS groups were significantly higher than those for the Rg3/PNS group; however, the CL values were lower than those for the Rg3/PNS group. This indicates that liposomes can slow the clearance rate of drugs and prolong their retention time in the plasma. The relative bioavailability of the formulation was reflected by the area under the curve (AUC_{0-t}).[53] The AUC_{0-t} values of Rg3, Rg1, and Rb1 in the Lip-Rg3/PNS group were 37.142, 74.556, and 25.162,

Table 1 Pharmacokinetic Parameters of Rg3 in Plasma After Intranasal Administration of Different Formulations (n=3)

Parameter	Unit	Rg3/PNS	Lip-Rg3/PNS	MM-Lip-Rg3/PNS
$t_{1/2}$	h	4.852±0.236	14.984±1.995***	18.880±1.309****$^{\#}$
C_{max}	μg·mL^{-1}	3.097±0.759	3.724±0.255	3.618±0.356
AUC_{0-t}	μg·mL^{-1}·h	8.720±0.452	37.142±2.215****	43.142±2.094****$^{\#}$
T_{max}	h	0.667±0.289	0.417±0.144	0.333±0.144
CL	L·h^{-1}·kg^{-1}	0.413±0.021	0.089±0.008****	0.070±0.003****
MRT	h	4.568±0.382	11.552±0.679****	14.467±0.999****$^{\#\#}$

Notes: The values were presented as the mean ± SD (n = 3). ***p <0.001, ****p < 0.0001 compared with Rg3/PNS; $^{\#}$p < 0.05, $^{\#\#}$p < 0.01 compared with Lip-Rg3/PNS.

Table 2 Pharmacokinetic Parameters of Rg1 in Plasma After Intranasal Administration of Different Formulations (n=3)

Parameter	Unit	Rg3/PNS	Lip-Rg3/PNS	MM-Lip-Rg3/PNS
$t_{1/2}$	h	4.007±0.214	15.493±2.626*	24.135±5.486***$^{\#}$
C_{max}	μg·mL^{-1}	9.516±1.732	21.275±1.103****	14.766±0.252**$^{\#\#}$
AUC_{0-t}	μg·mL^{-1}·h	39.427±1.726	74.556±5.683****	82.274±2.897****
T_{max}	h	0.250±0.000	0.160±0.000	0.250±0.000
CL	L·h^{-1}·kg^{-1}	0.119±0.005	0.059±0.007****	0.044±0.004****$^{\#}$
MRT	h	9.853±1.431	12.784±0.441*	15.732±0.340***$^{\#}$

Notes: The values were presented as the mean ± SD (n = 3). *p < 0.05, **p <0.01, ***p <0.001, ****p < 0.0001 compared with Rg3/PNS; $^{\#}$p < 0.05, $^{\#\#}$p <0.01 compared with Lip-Rg3/PNS.

Table 3 Pharmacokinetic Parameters of Rb1 in Plasma After Intranasal Administration of Different Formulations (n=3)

Parameter	Unit	Rg3/PNS	Lip-Rg3/PNS	MM-Lip-Rg3/PNS
$t_{1/2}$	h	3.810±0.285	10.445±0.752****$^{\#\#\#\#}$	17.422±1.687****$^{\#\#\#\#}$
C_{max}	μg·mL^{-1}	1.882±0.142	7.824±1.275***	4.582±0.027*$^{\#\#}$
AUC_{0-t}	μg·mL^{-1}·h	16.976±1.039	25.162±3.167*	32.672±2.083***$^{\#}$
T_{max}	h	0.500±0.000	0.500±0.000	0.160±0.000****$^{\#\#\#\#}$
CL	L·h^{-1}·kg^{-1}	0.236±0.015	0.155±0.019**	0.107±0.007****$^{\#}$
MRT	h	10.387±0.251	11.135±1.561	14.286±0.416****$^{\#\#\#}$

Notes: The values were presented as the mean ± SD (n = 3). *p <0.05, **p <0.01, ***p <0.001, ****p < 0.0001 compared with Rg3/PNS; $^{\#}$p < 0.05, $^{\#\#}$p < 0.01, $^{\#\#\#}$p < 0.001, $^{\#\#\#\#}$p < 0.0001 compared with Lip-Rg3/PNS.

respectively, in the MM-Lip-Rg3/PNS group, these values were 43.142 82.274, and 32.672, which were higher than the values in the Rg3/PNS group (8.720, 39.427, and 16.976). This proves that Lip-Rg3/PNS and MM-Lip-Rg3/PNS significantly improve bioavailability, suggesting a sustained release effect and extended drug presence in the plasma.

We further studied the distribution of these three formulations in the brain. As shown in Figure 8, the concentrations of Rg3, Rg1, and Rb1 in the brain of the Rg3/PNS group were not detected after 24 h. In contrast, Lip-Rg3/PNS and MM-Lip-Rg3/PNS remained in the brain for a longer time and were still detected at 48 h. Throughout the investigation, the concentrations of Rg3, Rg1, and Rb1 in the Lip-Rg3/PNS and MM-Lip-Rg3/PNS groups were higher than those in the Rg3/PNS group. This indicates that the brain uptake of both liposomes was higher than that of the free drugs. All three drug-time curves showed double peaks, potentially attributed to diverse brain entry pathways after intranasal administration, with some entering quickly via neural pathways and others indirectly entering through systemic circulation.[54] The $t_{1/2}$ values of Rg3, Rg1, and Rb1 in the Rg3/PNS group were 4.749 h, 3.752 h和2.335 h, respectively. Moreover, the $t_{1/2}$ values of both

liposome groups were significantly increased, especially in the MM-Lip-Rg3/PNS group, which increased to 34.892 h, 36.489 h和24.809 h, respectively. Compared to the Lip-Rg3/PNS and Rg3/PNS groups, the MRT of the MM-Lip-Rg3/PNS group also significantly increased, and the CL significantly decreased (Tables 4–6). Thus, MM-Lip-Rg3/PNS can significantly prolong the duration of drug action in the brain and is not easily degraded, which is crucial for maintaining therapeutic efficacy. By comparing AUC_{0-t}, it was found that the AUC_{0-t} of Rg3 in the MM-Lip-Rg3/PNS group was 2.04-fold and 12.91-fold higher than that of the Lip-Rg3/PNS and Rg3/PNS groups, with Rg1 being 1.38-fold and 4.43-fold higher, and Rb1 being 1.40-fold and 3.53-fold higher, respectively. This suggests that MM-Lip-Rg3/PNS can significantly increase drug bioavailability and distribution in the brain.

We also used Te, Re, Ce, and DTI targeting indices to study brain targeting by MM-Lip-Rg3/PNS (Tables 7–9). Te represents the degree of tissue targeting of the preparation; the larger the Te, the better the selectivity to the tissue. Re and Ce represent the tissue distribution of the formulation, where Re>1 and Ce>1 represent greater drug distribution in the tissue. DTI>1 indicates that the preparation is capable of brain targeting, and the larger the DTI, the stronger this

Table 4 Pharmacokinetic Parameters of Rg3 in Brain After Intranasal Administration of Different Formulations (n=3)

Parameter	Unit	Rg3/PNS	Lip-Rg3/PNS	MM-Lip-Rg3/PNS
$t_{1/2}$	h	4.749±0.055	12.970±1.760	34.892±9.050**##
C_{max}	μg·mL^{-1}	0.904±0.068	3.785±0.423	24.698±3.116****####
AUC_{0-t}	μg·mL^{-1}·h	5.928±0.418	37.598±1.463****	76.538±5.768****####
T_{max}	h	0.833±1.010	0.250±0.000	0.160±0.000
CL	L·h^{-1}·kg^{-1}	0.609±0.045	0.089±0.002****	0.034±0.001****
MRT	h	6.348±0.233	12.734±0.204****	13.698±1.046****

Notes: The values were presented as the mean ± SD (n = 3). **p <0.01, ****p < 0.0001 compared with Rg3/PNS; ##p < 0.01, ####p < 0.0001compared with Lip-Rg3/PNS.

Table 5 Pharmacokinetic Parameters of Rg1 in Brain After Intranasal Administration of Different Formulations (n=3)

Parameter	Unit	Rg3/PNS	Lip-Rg3/PNS	MM-Lip-Rg3/PNS
$t_{1/2}$	h	3.752±0.098	9.280±1.118*	36.489±3.208****####
C_{max}	μg·mL^{-1}	5.206±1.688	16.508±0.995****	15.289±0.505***
AUC_{0-t}	μg·mL^{-1}·h	28.531±2.255	91.752±1.135****	126.461±7.812****####
T_{max}	h	0.250±0.000	0.160±0.000****	0.080±0.000****####
CL	L·h^{-1}·kg^{-1}	0.165±0.014	0.050±0.001****	0.025±0.003****#
MRT	h	7.617±1.046	14.850±0.193***	15.778±1.203****

Notes: The values were presented as the mean ± SD (n = 3). *p <0.05, ***p <0.001, ****p < 0.0001 compared with Rg3/PNS; #p < 0.05, ####p < 0.001, ####p < 0.0001compared with Lip-Rg3/PNS.

Table 6 Pharmacokinetic Parameters of Rb1 in Brain After Intranasal Administration of Different Formulations (n=3)

Parameter	Unit	Rg3/PNS	Lip-Rg3/PNS	MM-Lip-Rg3/PNS
$t_{1/2}$	h	2.335±1.419	11.703±2.686*	24.809±3.308***##
C_{max}	μg·mL^{-1}	1.878±0.251	7.262±0.119****	8.950±0.232****###
AUC_{0-t}	μg·mL^{-1}·h	15.420±1.081	38.772±1.982****	54.387±0.187****####
T_{max}	h	0.273±0.196	0.08±0.000	0.250±0.000
CL	L·h^{-1}·kg^{-1}	0.260±0.019	0.098±0.003****	0.059±0.005****#
MRT	h	6.083±0.413	12.323±0.433****	14.967±0.762****##

Notes: The values were presented as the mean ± SD (n = 3). *p <0.05, ***p <0.001, ****p < 0.0001 compared with Rg3/PNS; #p < 0.05, ##p < 0.01, ####p < 0.001, ####p < 0.0001compared with Lip-Rg3/PNS.

Table 7 The Brain Tissues Targeting Parameters of Rg3 After Intranasal Administration of Different Formulations (n=3)

Formulation	Te	Re	Ce	DTI
Rg3/PNS	0.68			
Lip-Rg3/PNS	1.01	4.19	6.34	1.49
MM-Lip-Rg3/PNS	1.77	27.32	12.91	2.61

Table 8 The Brain Tissues Targeting Parameters of Rg1 After Intranasal Administration of Different Formulations (n=3)

Formulation	Te	Re	Ce	DTI
Rg3/PNS	0.72			
Lip-Rg3/PNS	1.23	3.17	3.22	1.71
MM-Lip-Rg3/PNS	1.54	2.94	4.43	2.13

Table 9 The Brain Tissues Targeting Parameters of Rb1 After Intranasal Administration of Different Formulations (n=3)

Formulation	Te	Re	Ce	DTI
Rg3/PNS	0.91			
Lip-Rg3/PNS	1.54	3.87	2.51	1.69
MM-Lip-Rg3/PNS	1.66	4.77	3.53	1.83

capability.[47,55,56] The results showed that Re>1 and Ce>1 in both the Lip-Rg3/PNS and MM-Lip-Rg3/PNS groups, indicating that liposomes were more widely distributed in the brain than free drugs. In addition, the order of Te values for Rg1, Rb1, and Rg3 in each formulation is MM-Lip-Rg3/PNS > Lip-Rg3/PNS > Rg3/PNS, indicating that compared with Rg3/PNS and Lip-Rg3/PNS, MM-Lip-Rg3/PNS exhibited a more obvious brain-targeting trend and entered the brain more easily, and the DTI values for each liposome group were calculated using Rg3/PNS as the control group. The results showed that the DTI values for Rg1, Rb1, and Rg3 in the Lip-Rg3/PNS and MM-Lip-Rg3/PNS group were all greater than 1, indicating that compared with Rg3/PNS, Lip-Rg3/PNS and MM-Lip-Rg3/PNS have stronger brain targeting ability.

In summary, MM-Lip-Rg3/PNS significantly prolonged the retention times of Rg3 and PNS in the body, increased the distribution of drugs in the brain.

Therapeutic Efficacy of MM-Lip-Rg3/PNS in MCAO Rats

We investigated the treatment efficiency of MM-Lip-Rg3/PNS using the experimental design shown in Figure 9A. TTC is a redox indicator that reacts with dehydrogenase in living tissues. This causes normal brain tissues to stain red, while ischemic infarcted tissues appear pale white due to enzyme inactivation.[57] As shown in Figure 9B, the brain tissues in the sham group were stained red, with no infarct location. The saline-treated group exhibited massive necrosis on the infarcted side of the brain. After the treatment, the infarct area decreased by varying degrees. The area of cerebral infarction was quantified using ImageJ, and the results showed that the infarct area in the MM-Lip-Rg3/PNS group was significantly reduced to 7.8%, compared to 35.3% in the saline group (Figure 9C). The Lip-Rg3/PNS and Rg3/PNS

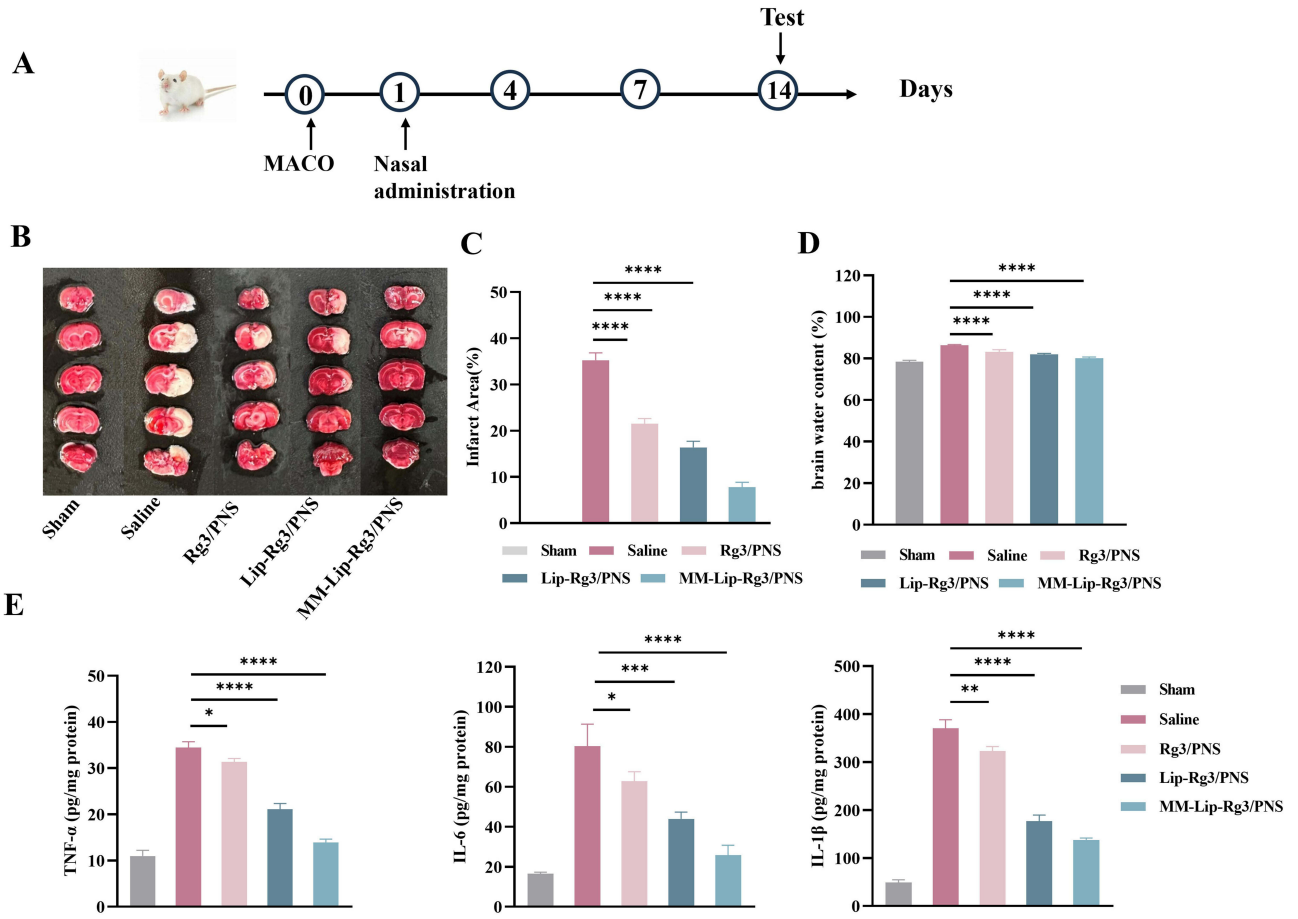

Figure 9 Cerebral ischemia treatment with different formulations 14 days in MCAO rats. (**A**) The experimental scheme. (**B**) Representative TTC staining images of coronal sections. (**C**) Quantified infarct ratio. (**D**) Quantified brain water content. (**E**) Expression of TNF-α, IL-6, and IL-10 in the ischemic brain after different treatment. The data were presented as the mean ± SD (n =3). ****p < 0.0001, ***p < 0.001, **p < 0.01, *p < 0.05.

groups also showed reduced infarct areas, but the effect was not as strong as that of the MM-Lip-Rg3/PNS group, with infarct areas of 16.4% and 21.5%, respectively. These results indicated that MM-Lip-Rg3/PNS had a stronger protective effect against brain injury. After an ischemic stroke, inflammatory reactions are accompanied by the production of a large number of inflammatory factors, further exacerbating brain tissue damage.[58] Common pro-inflammatory factors include TNF-α, IL-6, and IL-1β.[59] After drug treatment, the expression of inflammatory factors can be inhibited, especially by MM-coated liposomes, which can significantly reduce the production of TNF-α, IL-6, and IL-1β (Figure 9E). These results indicate that MM-Lip-Rg3/PNS can effectively target brain inflammatory sites and reduce brain damage. Ischemic stroke can lead to brain oedema and force brain volume to increase, thereby increasing risk.[60] Therefore, we evaluated the changes in brain water content before and after treatment. The results showed that compared with the sham group, the saline group showed a significant increase in brain water content and brain oedema (Figure 9D). After treatment with Rg3/PNS, Lip-Rg3/PNS, and MM-Lip-Rg3/PNS, water content decreased, with MM-Lip-Rg3/PNS showing the most significant therapeutic effect.

In vivo Safety Evaluation

According to H&E staining observation of tissue sections of the heart, liver, spleen, lung, kidney, and brain, there was no significant difference compared to the saline group (Figure 10). The results revealed the favorable safety of as-prepared MM-Lip-Rg3/PNS.

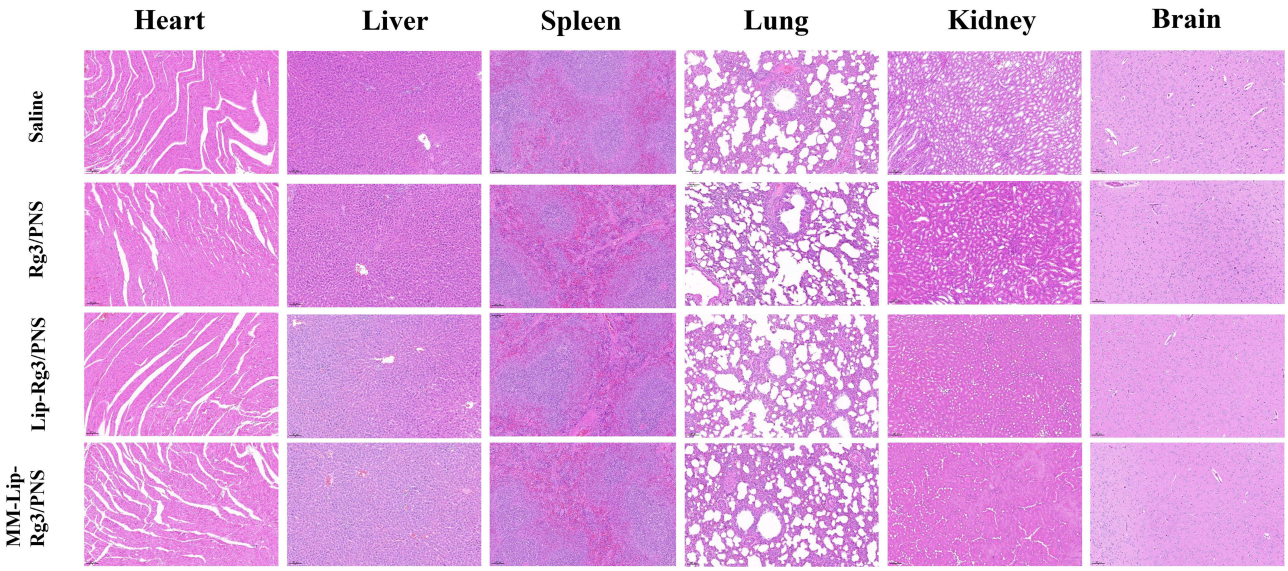

Figure 10 H&E staining of main organs including heart, liver, spleen, lung, kidney, brain. (scale bar = 100 μm).

Conclusions

This study aimed to transport Rg3 and PNS simultaneously to the ischemic site in the brain by encapsulating them in liposomes and coating the outer layer with a macrophage membrane, resulting in the design of biomimetic liposomes (MM-Lip-Rg3/PNS) for ischemic stroke treatment. Utilizing the intranasal administration pathway ensures a safe and swift entry of the drug into the brain. MM-Lip-Rg3/PNS exhibited favorable physical and chemical properties, including high EE, small particle size, and excellent stability. In vitro cell experiments showed that MM-Lip-Rg3/PNS inherits the biological characteristics of macrophages, avoiding macrophage phagocytosis. It actively responds to and binds with inflammatory brain endothelial cells, enhancing its ability to traverse the BBB. In vivo experiments showed that MM-Lip-Rg3/PNS can specifically target ischemic sites, even microglia, and accumulate in the ischemic hemisphere. This approach exhibits improved pharmacokinetic behavior, extended half-life, and increased drug bioavailability in the brain. It effectively alleviates brain inflammation, reduces brain oedema, and diminishes infarct volume, thereby alleviating brain damage and achieving effective therapeutic effects. Consequently, these biomimetic liposomes hold promise for introducing novel strategies in the treatment of ischemic stroke.

Data Sharing Statement

All data supporting the findings of this study are presented graphically or in tables in this manuscript.

Acknowledgments

This work was supported by the Ministry of Science and Technology of Jilin Province, China (201603048YY).

Funding

This research did not receive any specific grant from funding agencies in the public, commercial, or not-for-profit sectors.

Disclosure

The authors declare no competing interests in this work.

References

1. Bhaskar S, Stanwell P, Cordato D, Attia J, Levi C. Reperfusion therapy in acute ischemic stroke: dawn of a new era? *BMC Neurol*. 2018;18(1):8. doi:10.1186/s12883-017-1007-y
2. Yoo AJ, Pulli B, Gonzalez RG. Imaging-based treatment selection for intravenous and intra-arterial stroke therapies: a comprehensive review. *Expert Rev Cardiovasc Ther*. 2011;9(7):857–876. doi:10.1586/erc.11.56

3. Campbell BCV, De Silva DA, Macleod MR, et al. Ischaemic stroke. *Nat Rev Dis Primers*. 2019;5(1):5. doi:10.1038/s41572-019-0118-8
4. Jurcau A, Simion A. Neuroinflammation in cerebral ischemia and ischemia/reperfusion injuries: from pathophysiology to therapeutic strategies. *Int J Mol Sci*. 2022;23(1). doi:10.3390/ijms23010014
5. Selvaraj K, Gowthamarajan K, Karri V. Nose to brain transport pathways an overview: potential of nanostructured lipid carriers in nose to brain targeting. *Artif Cells Nanomed Biotechnol*. 2018;46(8):2088–2095. doi:10.1080/21691401.2017.1420073
6. Yu S, Li D, Shi A, et al. Multidrug-loaded liposomes prevent ischemic stroke through intranasal administration. *Biomed Pharmacother*. 2023:162. doi:10.1016/j.biopha.2023.114542
7. Alavian F, Shams N. Oral and intra-nasal administration of nanoparticles in the cerebral ischemia treatment in animal experiments: considering its advantages and disadvantages open access plus. *Curr Clin Pharmacol*. 2020;15(1):20–29. doi:10.2174/1574884714666190704115345
8. Laffleur F, Bauer B. Progress in nasal drug delivery systems. *Int J Pharmaceut*. 2021;607. doi:10.1016/j.ijpharm.2021.120994
9. Hanson LR, Frey WH. Intranasal delivery bypasses the blood-brain barrier to target therapeutic agents to the central nervous system and treat neurodegenerative disease. *BMC Neurosci*. 2008;9. doi:10.1186/1471-2202-9-S3-S5
10. Kim M, Lee Y, Lee M. Hypoxia-specific anti-RAGE exosomes for nose-to-brain delivery of anti-miR-181a oligonucleotide in an ischemic stroke model. *Nanoscale*. 2021;13(33):14166–14178. doi:10.1039/d0nr07516g
11. Schaefer ML, Böttger B, Silver WL, Finger TE. Trigeminal collaterals in the nasal epithelium and olfactory bulb: a potential route for direct modulation of olfactory information by trigeminal stimuli. *J Comp Neurol*. 2002;444(3):221–226. doi:10.1002/cne.10143
12. Wang SY, Li MH, Guo Y, et al. Effects of Panax notoginseng ginsenoside Rb1 on abnormal hippocampal microenvironment in rats. *J Ethnopharmacol*. 2017;202:138–146. doi:10.1016/j.jep.2017.01.005
13. Feng LD, Han F, Zhou L, et al. Efficacy and safety of (Xueshuantong) in patients with acute ischemic stroke (EXPECT) trial: rationale and design. *Front Pharmacol*. 2021:12. doi:10.3389/fphar.2021.648921
14. Zou S, Zhang MX, Feng LM, et al. Protective effects of notoginsenoside R1 on cerebral ischemia-reperfusion injury in rats. *Exp Ther Med*. 2017;14 (6):6012–6016. doi:10.3892/etm.2017.5268
15. Wu T, Jia ZH, Dong SF, et al. Saponins ameliorate leukocyte adherence and cerebrovascular endothelial barrier breakdown upon ischemia-reperfusion in mice. *J Vasc Res*. 2019;56(1):1–10. doi:10.1159/000494935
16. Im DS. Pro-resolving effect of ginsenosides as an anti-inflammatory mechanism of panax ginseng. *Biomolecules*. 2020;10(3):444. doi:10.3390/biom10030444
17. Cheng ZK, Zhang M, Ling CL, et al. Neuroprotective effects of ginsenosides against cerebral ischemia. *Molecules*. 2019;24(6):1102. doi:10.3390/molecules24061102
18. Wang J, Zeng L, Zhang Y, et al. Pharmacological properties, molecular mechanisms and therapeutic potential of ginsenoside Rg3 as an antioxidant and anti-inflammatory agent. *Front Pharmacol*. 2022:13. doi:10.3389/fphar.2022.975784
19. Li MY, Du CY, Guo N, et al. Composition design and medical application of liposomes. *Eur J Med Chem*. 2019;164:640–653. doi:10.1016/j.ejmech.2019.01.007
20. Ajeeshkumar KK, Aneesh PA, Raju N, et al. Advancements in liposome technology: preparation techniques and applications in food, functional foods, and bioactive delivery: a review. *Compr Rev Food Sci F*. 2021;20(2):1280–1306. doi:10.1111/1541-4337.12725
21. Guimaraes D, Cavaco-Paulo A, Nogueira E. Design of liposomes as drug delivery system for therapeutic applications. *Int J Pharmaceut*. 2021;601. doi:10.1016/j.ijpharm.2021.120571
22. Liu B, Zhang J, Liu Z, et al. Research on the preparation process of the cytarabine/daunorubicin dual-encapsulation liposome and its physico-chemical properties and performances in vitro/vivo. *Int J Pharm*. 2023;646:123500. doi:10.1016/j.ijpharm.2023.123500
23. Li YJ, Wu JY, Liu JH, et al. From blood to brain: blood cell-based biomimetic drug delivery systems. *Drug Deliv*. 2021;28(1):1214–1225. doi:10.1080/10717544.2021.1937384
24. Koupenova M, Kehrel BE, Corkrey HA, Freedman JE. Thrombosis and platelets: an update. *Eur Heart J*. 2017;38(11):785–791. doi:10.1093/eurheartj/ehw550
25. Fang RH, Kroll AV, Gao WW, Zhang LF. Cell membrane coating nanotechnology. *Adv Mater*. 2018;30(23). doi:10.1002/adma.201706759
26. Li RX, He YW, Zhang SY, Qin J, Wang JX. Cell membrane-based nanoparticles: a new biomimetic platform for tumor diagnosis and treatment. *Acta Pharm Sin B*. 2018;8(1):14–22. doi:10.1016/j.apsb.2017.11.009
27. Pang L, Zhang C, Qin J, et al. A novel strategy to achieve effective drug delivery: exploit cells as carrier combined with nanoparticles. *Drug Deliv*. 2017;24(1):83–91. doi:10.1080/10717544.2016.1230903
28. Wu HH, Zhang TY, Li N, Gao JQ. Cell membrane-based biomimetic vehicles for effective central nervous system target delivery: insights and challenges. *J Control Release*. 2023;360:169–184. doi:10.1016/j.jconrel.2023.06.023
29. Feng LS, Dou CR, Xia YG, et al. Neutrophil-like cell-membrane-coated nanozyme therapy for ischemic brain damage and long-term neurological functional recovery. *Acs Nano*. 2021;15(2):2263–2280. doi:10.1021/acsnano.0c07973
30. Yan JJ, Fei WD, Song QQ, et al. Cell membrane-camouflaged PLGA biomimetic system for diverse biomedical application. *Drug Deliv*. 2022;29 (1):2296–2319. doi:10.1080/10717544.2022.2100010
31. Zhang RT, Wu SQ, Ding Q, et al. Recent advances in cell membrane-camouflaged nanoparticles for inflammation therapy. *Drug Deliv*. 2021;28 (1):1109–1119. doi:10.1080/10717544.2021.1934188
32. Li C, Zhao ZH, Luo YF, et al. Macrophage-disguised manganese dioxide nanoparticles for neuroprotection by reducing oxidative stress and modulating inflammatory microenvironment in acute ischemic stroke. *Adv Sci*. 2021;8(20). doi:10.1002/advs.202101526
33. Jian ZH, Liu R, Zhu XQ, et al. The involvement and therapy target of immune cells after ischemic stroke. *Front Immunol*. 2019;10:10. doi:10.3389/fimmu.2019.02167
34. Gelderblom M, Leypoldt F, Steinbach K, et al. Temporal and spatial dynamics of cerebral immune cell accumulation in stroke. *Stroke*. 2009;40 (5):1849–1857. doi:10.1161/Strokeaha.108.534503
35. Cai W, Hu MY, Li CY, et al. FOXP3+macrophage represses acute ischemic stroke-induced neural inflammation. *Autophagy*. 2023;19(4):1144–1163. doi:10.1080/15548627.2022.2116833
36. Zhang H. Thin-Film hydration followed by extrusion method for liposome preparation. *Methods Mol Biol*. 2017;1522:17–22. doi:10.1007/978-1-4939-6591-5_2

37. Wu HH, Jiang XC, Li YS, et al. Engineering stem cell derived biomimetic vesicles for versatility and effective targeted delivery. *Adv Funct Mater*. 2020;30(49). doi:10.1002/adfm.202006169
38. Hayes BH, Tsai RK, Dooling LJ, et al. Macrophages show higher levels of engulfment after disruption of interactions between CD47 and the checkpoint receptor SIRPα. *J Cell Sci*. 2020;133(5). doi:10.1242/jcs.237800
39. Perego C, Fumagalli S, Zanier ER, et al. Macrophages are essential for maintaining a M2 protective response early after ischemic brain injury. *Neurobiol Dis*. 2016;96:284–293. doi:10.1016/j.nbd.2016.09.017
40. Liu W, Lu HW, Rao XY, et al. Enhanced treatment for cerebral ischemia-reperfusion injury of puerarin loading liposomes through neutrophils-mediated targeted delivery. *Nano Res*. 2021;14(12):4634–4643. doi:10.1007/s12274-021-3395-y
41. Jiang YY, Liu CQ, Zhai WC, et al. The optimization design of lactoferrin loaded HupA nanoemulsion for targeted drug transport via intranasal route. *Int J Nanomed*. 2019;14:9217–9234. doi:10.2147/Ijn.S214657
42. Askarizadeh A, Barreto GE, Henney NC, Majeed M, Sahebkar A. Neuroprotection by curcumin: a review on brain delivery strategies. *Int J Pharmaceut*. 2020;585. doi:10.1016/j.ijpharm.2020.119476
43. Alexander A, Agrawal M, Uddin A, et al. Recent expansions of novel strategies towards the drug targeting into the brain. *Int J Nanomed*. 2019;14:5895–5909. doi:10.2147/Ijn.S210876
44. Brown RC, Morris AP, O'Neil RG. Tight junction protein expression and barrier properties of immortalized mouse brain microvessel endothelial cells. *Brain Res*. 2007;1130(1):17–30. doi:10.1016/j.brainres.2006.10.083
45. Li GL, Simon MJ, Cancel LM, et al. Permeability of endothelial and astrocyte cocultures: blood-brain barrier models for drug delivery studies. *Ann Biomed Eng*. 2010;38(8):2499–2511. doi:10.1007/s10439-010-0023-5
46. Zhang YD, He JL, Shen L, et al. Brain-targeted delivery of obidoxime, using aptamer-modified liposomes, for detoxification of organophosphorus compounds. *J Control Release*. 2021;329:1117–1128. doi:10.1016/j.jconrel.2020.10.039
47. Jiang YY, Jiang YC, Ding ZY, Yu Q. Investigation of the "Nose-to-Brain" pathways in intranasal HupA nanoemulsions and evaluation of their in vivo pharmacokinetics and brain-targeting ability. *Int J Nanomed*. 2022;17. doi:10.2147/Ijn.S369978
48. Li Y, Zhang MM, Li SY, et al. Selective ischemic-hemisphere targeting Ginkgolide B liposomes with improved solubility and therapeutic efficacy for cerebral ischemia-reperfusion injury. *Asian J Pharm Sci*. 2023;18(2). doi:10.1016/j.ajps.2023.100783
49. Wang C, Yang XW, Jiang YX, et al. Targeted delivery of fat extract by platelet membrane-cloaked nanocarriers for the treatment of ischemic stroke. *J Nanobiotechnol*. 2022;20(1). doi:10.1186/s12951-022-01461-2
50. Yilmaz G, Granger DN. Leukocyte recruitment and ischemic brain injury. *Neuromolecular Med*. 2010;12(2):193–204. doi:10.1007/s12017-009-8074-1
51. Arumugam TV, Salter JW, Chidlow JH, et al. Contributions of LFA-1 and Mac-1 to brain injury and microvascular dysfunction induced by transient middle cerebral artery occlusion. *Am J Physiol-Heart C*. 2004;287(6):H2555–H2560. doi:10.1152/ajpheart.00588.2004
52. Han Y, Gao C, Wang H, et al. Macrophage membrane-coated nanocarriers Co-Modified by RVG29 and TPP improve brain neuronal mitochondria-targeting and therapeutic efficacy in Alzheimer's disease mice. *Bioact Mater*. 2021;6(2):529–542. doi:10.1016/j.bioactmat.2020.08.017
53. Tang H, Xie YZ, Zhu M, et al. Estrone-conjugated PEGylated liposome co-loaded paclitaxel and carboplatin improve anti-tumor efficacy in ovarian cancer and reduce acute toxicity of chemo-drugs. *Int J Nanomed*. 2022;17:3013–3041. doi:10.2147/Ijn.S362263
54. Keller LA, Merkel O, Popp A. Intranasal drug delivery: opportunities and toxicologic challenges during drug development. *Drug Deliv Transl Re*. 2022;12(4):735–757. doi:10.1007/s13346-020-00891-5
55. Xiang Y, Long Y, Yang QY, et al. Pharmacokinetics, pharmacodynamics and toxicity of Baicalin liposome on cerebral ischemia reperfusion injury rats via intranasal administration. *Brain Res*. 2020:1726. doi:10.1016/j.brainres.2019.146503
56. Lu JQ, Li R, Mu BS, et al. Multiple targeted doxorubicin-lonidamine liposomes modified with -hydroxybenzoic acid and triphenylphosphonium to synergistically treat glioma. *Eur J Med Chem*. 2022:230. doi:10.1016/j.ejmech.2021.114093
57. Benedek A, Móricz K, Jurányi Z, et al. Use of TTC staining for the evaluation of tissue injury in the early phases of reperfusion after focal cerebral ischemia in rats. *Brain Res*. 2006;1116(1):159–165. doi:10.1016/j.brainres.2006.07.123
58. Tirandi A, Sgura C, Carbone F, Montecucco F, Liberale L. Inflammatory biomarkers of ischemic stroke. *Intern Emerg Med*. 2023;18(3):723–732. doi:10.1007/s11739-023-03201-2
59. Yang CJ, Hawkins KE, Doré S, Candelario-Jalil E. Neuroinflammatory mechanisms of blood-brain barrier damage in ischemic stroke. *Am J Physiol-Cell Ph*. 2019;316(2):C135–C153. doi:10.1152/ajpcell.00136.2018
60. Han WX, Song Y, Rocha M, Shi YJ. Ischemic brain edema: emerging cellular mechanisms and therapeutic approaches. *Neurobiol Dis*. 2023;178. doi:10.1016/j.nbd.2023.106029